UNIVERSITY OF OKLAHOMA

GRADUATE COLLEGE

DEVELOPMENT OF NANOPARTICLE MEMBRANE ENHANCED NANOCOMPOSITES WITH SENSING FUNCTION

A THESIS

SUBMITTED TO THE GRADUATE FACULTY

in partial fulfillment of the requirements for the

Degree of

MASTER OF SCIENCE

By

WANRU SHANG
Norman, Oklahoma
2016

DEVELOPMENT OF NANOPARTICLE MEMBRANE ENHANCED NANOCOMPOSITES WITH SENSING FUNCTION

A THESIS APPROVED FOR THE
SCHOOL OF AEROSPACE AND MECHANICAL ENGINEERING

BY

_____
Dr. Yingtao Liu, Chair

_____
Dr. M. Cengiz Altan

_____
Dr. Mrinal Saha

Acknowledgements

I would like to express my sincere gratitude and thanks to my advisor Dr. Yingtao Liu for his extensive support, invaluable advice, and constant encouragement during my studies, and his insightful guidance as both advisor and friend.

I also thank Dr. Altan and Dr. Saha, for serving on my thesis committee, and their suggestions and assistance during the preparation of this thesis. Special thanks to Dr. Allen and Dr. Mistree for being my considerate mentors with unconditional concern and support, enlightening both my career and life path.

A sincere appreciation goes to all my co-workers in SMIS lab, Shoieb, Yi, Jingyu, Mark, Wenyuan, and all members in SRL lab for their help and meaningful help to this thesis, and made my experimental work and studies rewarding and enjoyable. I would like to express my sincere gratitude for AME department for financial support and encouraging academic environment.

Lastly, I would like to thank my parents for their unconditional love and unflinching support to my academic endeavors without which I would not be where I am today. Thank my friends Ling, Andrew, Jiehao, Hong, Trey, and friends back in China, for their encouragement and company throughout my life and education. I appreciate the precious support and love from my boyfriend Brax, his dad Kevin, and his family to help me go through all difficult time

studying and surviving in this new environment. Thanks to his profound love, I grew up to be strong and mature.

Table of Contents

List of Tables

List of Figures

Abstract

Damage and load sensing is rapidly advancing as driven by vast applications in aerospace and mechanical structures. However, most previous research focused on the improvement of material properties for sensing applications. Limited work balanced the sensor design and material innovation for real-time strain sensing. In this paper nanocomposite membranes are proposed for the strain sensing. The micro-scale morphology and structures are first experimentally characterized. Both the fabrication process for BuckyPapers and nanocomposites are investigated to obtain the optimal sensing capabilities. The sensing function is achieved by correlating the piezo-resistance variations to the strain applied on the sensing area. Due to the conductive network formed and the tunneling resistance change in neighboring nanoparticles, the electrical resistance changes will show a clear correlation with the load conditions. The sensitivity of the composite sensor can reach around 0.9, while the optimal strain range for practical applications is between 0.1 - 0.31%. In this range, composites show elastic deformation while the electrical resistance possess closely linear response to the strain applied. The characterized membrane structures have the potential to be further applied to continuously monitor impact loads, especially focusing on low velocity barely visible damage in composites.

Chapter 1: Introduction

Since the discovery of carbon nanotubes (CNTs) [1], the application of CNTs and related materials have been active research fields over the last decade because of their attractive electrical, mechanical, and thermal properties [2]. According to the percolation theory, CNTs provide three-dimensional conductive paths. Since the electrical paths are made up of conductive inclusions in the direct contact, CNTs show excellent potential in electrical applications. CNTs have been demonstrated to be the promising reinforcement material for advanced structural and multifunctional composites with high-performance, and evoked great interest in polymer-based composites research. The addition of CNTs can proportionally transfer their unique and excellent properties into polymers and bring about substantial advanced improvements such as strength, electrical and thermal conductivity, and electromagnetic interference shielding. Among thermosetting polymers, epoxy-based system is preferable for structural applications, like automotive and electronics, for their excellent mechanical properties for structural stability, and heat and chemical resistance. Based on knowledge, the ultralow threshold was obtained that the CNTs concentration between 0.5 - 1 wt. % in epoxy to achieve the insulation-to-conductor transition [3, 4]. The effects of mechanical deformation on the electrical properties of CNTs was revealed by using the tip of an atomic force microscope (AFM) to manipulate CNTs [5], which indicated that CNTs have the potential to be the candidate of sensing applications.

1.1 Introduction of CNTs and their advantages

There are two types of CNTs, single-wall carbon nanotubes (SWNTs) and multi-wall carbon nanotubes (MWNTs). SWNTs can be considered as a sheet of graphite that has been rolled into a tube. MWNTs are composed of a number of SWNTs held together with weak Van der Waals forces, as shown in Figure 1.1 (a). Typically, one individual MWNT tube consists of 15-35 rolled layers of graphene [6]. Due to different ways to roll the graphite up, the twist results in different nanostructures and chirality, as shown in Figure 1.1 (b). The chirality has significant implications on the electronic properties. CNTs can show either metallic or semiconducting, even though graphite is considered to be semi-metal [7].

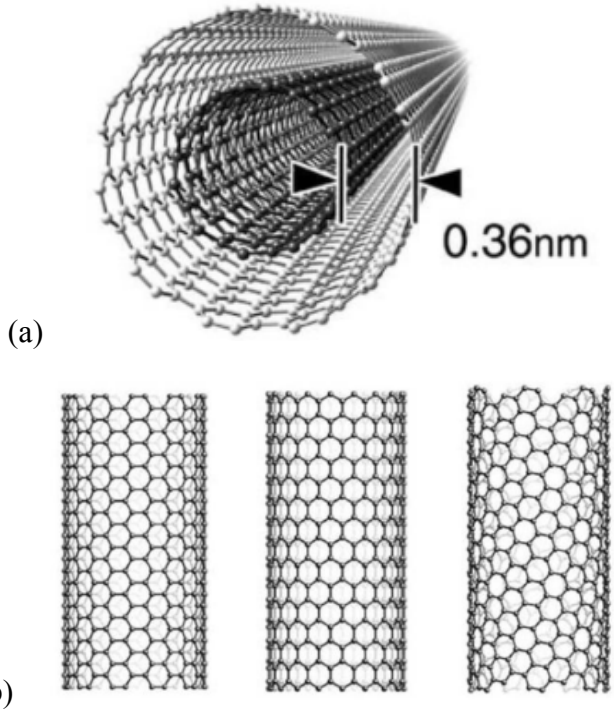

Figure 1.1: (a) Two-layer MWNT; (b) SWNTs in the armchair form (left), zigzag form (center), and helical form (right) [8]

SWNTs possesses the highest tensile modulus and ultimate tensile load. The Young's modulus can reach around 1TPa [9]. The elastic modulus, Poisson's ratio and bulk modulus were found out to be strongly dependent on the tube radius [10, 11]. When it comes to MWNTs, the elastic properties are the same for all nanotubes when the radius of out-most layer is larger than 1 nm [12], which is due to the failure of MWNTs happens when the inner tubes are pulled out from the outer tubes before the outmost layer starts to fail [13].

In 1995, Chico et al. [14] carried out the theoretical study about the electrical properties of CNTs and revealed the potential of CNTs to be used in blocks of nanoscale semiconductor devices. They introduced the pentagon-heptagon pair defects into the hexagonal network of SWNTs, which provided an interface between tubule segments of different helicities with different electronic gaps, and proposed a new type of metal/semiconductor or semiconductor/semiconductor heterojunction. This defect resulted in a global change in the helicity of the tube and furthermore altering electronic structure.

The defects are inevitable in the volume production of CNTs, which results in the strength of CNTs in the macro scale may not be able to match with that of a SWNT. However, the interface coupling effect results from the high specific surface area may compensate the effects of defects. From this perspective, compared to Carbon nanofiber, the strength of knotted CNTs doesn't decrease.

Since the discovery of CNTs in 1990s, both theoretical and experimental

approaches have been carried out to reveal the effects of mechanical deformation on the electrical resistance of CNTs. In 1996, Crespi et al. [14, 15] set up models on CNTs, providing a novel class of elemental heterojunctions. They discovered that pentagon-heptagon pair defects into the hexagonal network of a SWNT could change the helicity of the tube and alter its electronic structure. Based on this calculation, they proposed metal/semiconductor or semiconductor/semiconductor junctions that could be built blocks of nanoscale semiconductor devices. Later, in 1997, their calculation [16] indicated that bond rotation defects closed the gap in large-gap nanotubes, opened the gap in small-gap nanotubes, and increased the density of states in metallic nanotubes. These defects resulted in stronger one-dimensional effects than defect-free metallic nanotubes. They found the CNTs dramatic variations in electronic structure upon perturbation of the sp^2 framework, which could be used to tune the electronic, transport, and field emissive properties of sp^2-based CNTs.

In 1997, Kane et al. [17] derived a model to analyze the effects of tubule size, shape, symmetry and inhomogeneous shape deformation on nominally metallic armchair tubes. Their model analyzed the local twists and bends of tubes could change the π electrons propagating along the tubes, which further influenced the resistance.

In 1998, Rochefort et al. [18] moved forward to the effects of bending on σ-bonds and mixture of σ-bonds and π-bonds. The bending angle increased from 0° to 30°, 45° and 60°, and the drastic structural deformation occurred

from 45° to 60°. Their calculation stated that bending increased $sp^2 - sp^3$ rehybridization, which resulted in the change of electrical transport properties of CNTs.

In 1997, Tans et al. [19] confirmed the theoretical predictions that SWNTs act as genuine quantum wires by electrical transport measurements on the individual SWNT. Their results also indicated that the electronic states were extended and had a strong one-dimensional nature. Later, in 1998, the first multi-probe measurement on individual SWNT was obtain by Bezryadin et al. [20] and they came to the conclusion that tube could be considered as a chain of 1D quantum wires connected in series. When it came to MWNTs, Langer et al. [21] carried out electrical resistance measurements on an individual MWNT and supported the theoretical prediction that isolated MWNTs behave as disordered mesoscopic 2D graphite sheets. They reported that the electrical transport in a MWNT was governed by typical electron interference effects occurring in disordered conductors with a reduced dimensionality.

Besides the theoretical researches, experiments were carried out later on. In 1997, Bockrath et al. [22] measured the electrical properties of individual bundles of SWNTs and explained the results based on their Coulomb blockade model, instead of the individual tube which was mentioned in theoretical researches.

In 1999, Paulson et al. [23] applied strain with an AFM probe to MWNTs to investigate the response. Their results showed that tubes were broken by

enough force applied, without any change in the resistance until the tube failed. It indicated that when tubes behaved as elastic deformation, the resistance remained unchanged while the resistance change occurred until fracture or plastic deformation. They also pushed the ends of broken tubes into each other and the resistance increased by 10%. This would give an inspiration for BPs that the contact tubes could remain conductive without big changes in resistance.

Nardelli et al. [24] also reported their experiments on the effects of mechanical deformations on electrical properties of CNTs. They came to the conclusion that bending, defects, and tube-tube contacts strongly modified the electrical behavior of CNTs. Topological defects always increased the resistance of metallic nanotubes to an extent. Their results also showed that putting open-ended CNTs close to join each other can form conducting electrical contacts again.

In 2000, Tombler et al. [5] revealed the effects of mechanical deformation on the electrical properties of CNTs by using the tip of an AFM to manipulate a SWNT. To avoid contact resistance change, they applied AFM tips to deflect reversibly the suspended SWNTs, which could be considered as an elastic string. Importantly, both the mechanical deformation and electrical conductance of the SWNT are highly reversible. The results showed that the conductance of an SWNT sample reduced by two orders of magnitude when deformation came to 80 nm, which may due to the change of the formation from

local sp^2-bonds to nearly sp^3-bonds caused by the pushing force from the tip, according to the order-N non-orthogonal tight-binding molecular-dynamic simulations. Since the π electrons were mainly responsible for conduction, during the simulation, the π-electrons density was found a significant decrease, which contributed to the decrease in the SWNTs' resistance conductivity. The conjuncture could be made as a highly kinked SWNT, stabilized by Van der Waals force, possessing more significant electrical conductance change, when applied force, than a straight tube.

As stated above, both theoretical and experimental researches revealed that CNTs possess the reversible electromechanical characteristics. According to the percolation theory, CNTs provide three-dimensional conductive paths. Since the electrical paths are made up of conductive inclusions in the direct contact, CNTs show excellent potential in electrical applications [25].

The advantages of CNTs evoked the research interests to add CNTs into polymer based composites [7]. The addition of CNTs can proportionally transfer their unique and excellent properties into polymers and bring about substantial advanced improvements such as strength, electrical and thermal conductivity, electromagnetic interference shielding, etc. [26].

It has been expected that CNTs could play a role as an excellent reinforcement in polymer composites [27]. For nearly a decade of research, a number of studies have been conducted [28].

1.2 CNT composites

There are two types of polymers: thermoset and thermoplastic polymers. Thermoset polymers contain cross-link network, which forms irreversible chemical bonds. They can only be heated and shaped once because of this three-dimensional network of bonds, and in another words, they can't be recycled. On the other hand, thermoplastic polymers have no chemical bonds formed during the curing process, which makes them completely reversible. Due to the differences in the curing process, these two plastics show definitely different mechanical properties. Thermoset polymers possess the stronger chemical resistance, heat resistance and structural integrity than thermoplastic polymers. Those properties make them a better candidate for electronic devices and structural materials. It is worth noting that, since thermoset polymers are stronger than thermoplastic polymers, they are generally brittle.

Epoxy resin is one type of the thermoset polymers. Among thermoset polymers, epoxy-based systems are preferable for structural applications, like automotive and electronics, for their excellent mechanical properties for structural stability, and heat and chemical resistance. Epoxy resin is known as better polymer matrix compared with other polymer resins because CNTs are better dispersed in it.

There have been a lot of studies for the CNTs/epoxy composites with the increased demand for multifunctional advanced nanostructured composites [29, 30]. For example, CNTs were used to fabricate the CNTs flexible thin film

composite materials with high transparency and electrical conductivity, due to the outstanding electrical conductivity [31].

Yan et al. [32] employed AmPy-12 to achieve the highest functionalization efficiency for SWNTs in terms of dispersion. The AmPy-12 interacted with SWNTs non-covalently but bonded chemically to the epoxy matrix. Their results showed that the composite with only 0.3 wt. % SWNTs displayed an increase of 54% and 27% in tensile strength and Young's modulus, respectively, over neat resin. Besides, a low electrical percolation threshold of 0.1 wt. % SWNTs and improved thermal properties were also observed.

Felisberto et al. [33] indicated that the aligned CNTs showed better performance than randomly oriented ones. The percolation threshold of the epoxy resin-based composite could go down to 0.06 wt. % for aligned CNTs compared to randomly oriented CNTs (0.5 wt. %). Allaoui et al. [3] also found out the saturation effect of CNTs in epoxy mechanical properties. They suggested that if CNTs were randomly distributed, it would not be helpful to use high CNTs concentrations to improve the mechanical properties of the composites.

Allaoui et al. [3] obtained that the CNTs concentration between 0.5 - 1 wt. % in epoxy achieved the insulator-to-conductor transition. The Young's modulus and the yield strength had been doubled and quadrupled for composites with respectively 1 and 4 wt. % nanotubes, compared to the pure resin matrix samples. Conductivity measurements on the composite samples

showed that the insulator-to-conductor transition took place for nanotubes concentration between 0.5 - 1 wt. %.

Rajagopal [34] fabricated CNT/polymer composites using non-covalently functionalized and soluble SWNTs (PPE-functionalized SWNTs), which shortened the sonication time. The low percolation threshold was achieved as 0.05 - 0.1 wt. % SWNTs. The conductivity reached 6.89 S/m at 7 wt. % loading. Functionalization allowed the homogeneous dispersion of SWNTs in various polymer matrices.

Han et al. [35] fabricated self-sensing MWNTs/cement composites that could be used for traffic monitoring. They explored the piezo-resistive properties of CNTs to detect the mechanical stresses induced by traffic flow. Both laboratory tests and field tests presented sensitive and stable response to repeated compressive and impulsive loading. This work has remarkable potential for traffic flow detection, weigh-in-motion measurement and vehicle speed detection.

Even though, sufficiently high electrical conductivity has been achieved as introduced above, higher conductivities are still required especially for the applications like aerospace applications.

To develop innovative CNTs-based nanocomposites, there are two most relevant issues concerned: i) the effective dispersion of CNTs [36], ii) the strong interfacial bonding to create the strong adhesion to the polymeric matrix. These two issues may not be related or achieved at the same time. Especially, the

second one – strong adhesion affects the mechanical properties more than the electrical conductivity.

It is reported that dispersion is the dominate factor to influence the electrical and thermal conductivity because epoxy composites with better CNTs dispersion yield much higher electrical and thermal conductivity [37], which is explained as well dispersed CNTs are able to form more effective conductive paths. Furthermore, Guadagno et al. [38] studied the effect of improved dispersion caused by -COOH functionalization, on the electrical properties. Their results showed that the -COOH modification had stronger effect at low temperature and actually had no improvements on the composites stiffness.

Based on knowledge, no samples with higher than 4% [3, 38] concentration can be fabricated successfully due to the high viscosity of epoxy resin and the aggregation of CNT bundles.

Li et al. [39] addressed another factor that in the CNTs-based nanocomposites, the tunneling resistance played a dominant role in electrical conductivity of composites and the maximum tunneling distance was about 1.8 nm. What's more, with the layer thickness increasing, the tunneling resistance increased very rapidly. Their results indicated that the electrical conduction depended strongly on the content of CNTs, the contact resistance played a dominant role in the electrical conduction of CNTs-based nanocomposites. At the certain content of CNTs, the contact resistance played the dominant role in

electrical conduction. This could explain that the reported electrical conduction varies may due to the different CNTs network.

Some of these composites exhibit a fairly linear and reversible electrical resistance behavior. As opposed to the intrinsic piezo-resistive effect found affecting the electric properties of an individual CNT, it is reported that the piezo-resistive properties of CNTs-based composites are controlled by interactions between the CNTs [40].

Because of the Van der Waals force, CNTs tend to aggregate into bundles. Therefore, the uniform dispersion and distribution of CNTs in host materials are essential for developing the nanocomposites [41, 42]. To avoid the fabrication difficulties, CNTs have been fabricated to membrane structures and used in sensing application. Such membranes are also referred as BuckyPapers (BPs) in literature.

Here is one concept to clarify first. In this work, we define BPs as a sheet of CNTs. When it is applied to fabricate composites, the shape as a sheet of paper remains. In the work of Petra et al. [43], they claimed the composites were made from BP films, which I personally was not in favor of, because basically, they dispersed 1 wt. % functionalized CNTs into polymer, where there was no sheet of paper anymore.

Table 1.1 showed the brief summary and comparison of CNTs-based composites from former researchers.

Table 1.1: Brief review of CNTs-based composites

Author	Electrical Percolation Threshold	Functionalization	Improvement
2002 Allaoui et al. [3]	0.5 - 1 wt. % CNTs/epoxy	N/A	With 1 wt. % CNTs, Young's modulus and the yield strength have been doubled and quadrupled, respectively.
2003 Rajagopal [34]	0.045 wt. % PPE-SWNTs/Poly-carbonate	Poly(phenyleneethynylene)s (PPE)-functionalized SWNTs	The conductivity reaches 6.89 S/m at 7 wt. % loading
2009 Petra et al. [43]	0.5 wt. % MWNTs/poly-carbonate	Plasma functionalized MWNTs	N/A
2012 Yan et al. [32]	0.1 wt. % AmPy-12-SWNTs/epoxy	Amino-containing pyrenen derivatives (AmPys) functionalized SWNTs	0.3 wt. % SWNTs increase 54 % in tensile strength
2012 Felisberto et al. [33]	0.06 wt. % (aligned CNT) 0.5 wt. % (randomly oriented CNTs)	N/A	The achieved conductivity was 1.4×10^{-5} S/m

It is reported that the dispersion state of CNTs may influence the storage modulus, viscosity, electrical conductivity [44, 45]. With the CNTs loading increasing, the storage modulus of the composites dramatically increases. This can be explained as the particle-particle interactions and particle-fluid interactions increase due to the cylindrical shape with high aspect ratio of CNTs. The well dispersed CNTs-based nanocomposites show better performance in tensile strength, storage modulus, loss modulus, and complex viscosity, which has been explained that the agglomerates in the poorly dispersed CNTs act as large particles with the increase of the CNTs loading. What's more, the poorly dispersed CNTs exhibit stronger non-Newtonian behavior, which means it has, from a rheological point of view, a more solid-like behavior. Especially, dispersion is the dominate factor to influence the electrical and thermal conductivity due to the results that epoxy composites with better CNTs dispersion yield much higher electrical and thermal conductivity [37], which has been explained as well dispersed CNTs are able to form more effective conductive paths. Based on knowledge, no samples with higher than 4% [3, 38] concentration can be fabricated successfully due to the high viscosity of epoxy resin and the aggregation of CNTs bundles.

Therefore, the uniform dispersion and distribution of CNTs, as well as improvement of CNTs concentration, in host materials are essential for developing the nanocomposites [42, 46].

Based on the discussion, CNTs mats or BPs have relatively smaller contact resistance and results in much higher conductivity. In CNTs mats or BPs, the intrinsic resistance of CNTs can contribute more. This is the motivation for this work to investigate the properties and applications for BPs embedded nanocomposites and electrical sensing functions.

BPs is a sheet of porous internal structure of CNTs. It is one method to develop CNTs-based nanocomposites with high performance. In next section, advantages and applications of BPs will be introduced.

By making CNTs into BP membranes, the dispersion issue can be avoided because CNTs don't have to be dispersed into epoxy matrix since they are already formed into a uniform sheet. In addition, embedding BPs into epoxy can significantly improve the CNTs concentration in the nanocomposites. It has been reported that BP membranes possess the advanced properties of highly porosity, flexibility and electrical conductivity [41, 47]. Recently, BPs/polymer nanocomposites have received high recognition in various applications, such as water filters, temperature sensing, strain sensing, electrode support material for biofuel cells and biosensors, electrostatic dissipation, electrostatic painting and coating, electromagnetic interference shielding, substrates for never cell growth, and artificial muscles [34, 48-55].

1.3 Introduction of BPs and their advantages

BP membranes can be made by SWNTs, MWNTs, and mixed nanomaterials such as MWNTs and carbon nanofibers (CNFs) [42, 56, 57]. It

has been reported that the BP membranes possess the advanced properties of highly porosity, flexibility and electrical conductivity [46, 50].

Liu et al. [58] reported that under 39.1 wt. % MWNTs content, the tensile performance increased with the content of CNTs. When it reached 39.1%, the Young's modulus could reach 15.1 GPa, which was 492% higher than the neat epoxy. When it went beyond 39.1%, the epoxy couldn't fill, soak, or imbue totally, which led to lean material and crack flaws. They also found out that, brittle epoxy improved more than ductile ones, which indicated that the epoxy crossing network influenced more than adhesion bonding between epoxy and BPs.

The composites fabricated by Han et al. [59] containing 42.6 vol. % CNTs-BP coated by thermoplastic polyurethane exhibited simultaneous improvements in stiffness (up to 6 GPa), strength (up to 123 MPa), ductility (up to 30%), and toughness (up to 36 MJ/m^3), compared to those of the as-prepared IBP. The results revealed that ductile polymers were very promising matrix in balancing the key mechanical properties of BPs, which were beyond the commonly used brittle thermosets, e.g. epoxy resin.

Li et al. [60] fabricated epoxy nanocomposites with CNTs skeleton which achieved electricity up to 1000 S/cm and Young's modulus up to 30 GPa. It is found that the thicknesses of the nanocomposite films could be easily controlled in the range of 0.5 – 3 μm. The consequent measurements revealed that the mechanical and electrical properties of SWNTs/epoxy nanocomposite films

could be tailored in a quite wide range. For examples, the Young's modulus of nanocomposite films can be tuned from 10 to 30 GPa, and the electrical conductivity can be ranged from 1000 S/cm to be insulated.

Khan [61] found that the hybrid films of CNTs and nanographite platelets had superior properties over neat CNTs-based BPs or nanographite-based BPs. They prepared mixed dispersions of SWNTs and nanographite/graphene in the solvent N-methyl pyrrolidone. Mechanical measurements showed the hybrids stronger and stiffer than nanotube or graphene-only films, reaching strength and stiffness of 38 MPa and 4.8 GPa, respectively for the sample with 20 wt. % graphene. In addition, the hybrid films were more electrically conductive than the nanotube or graphitic-only films reaching a DC conductivity of 2×10^4 S/m for the 70 wt. % nanographite/graphene sample.

Table 1.2: Brief review of BPs/epoxy composites

Author	Composites	Improvement
2010 Khan [61]	SWNTs/nanographite/graphene-based BPs/epoxy	Conductivity reached 2×10^4 S/m with 70 wt. % BPs. strengths and stiffness reached 38 MPa and 4.8 GPa, respectively.
2011 Li et al. [60]	SWNTs-based BPs/epoxy	Young's modulus of nanocomposite films can be tuned from 10 to 30 GPa, and the electrical conductivity ranged from 1000 S/cm to be insulated.
2014 Han [59]	42.6 vol. % CNTs-BPs coated by different polymers	Ductile polymers are very promising matrix than brittle matrix

Dharap et al. [62] investigated the strain sensing capability of SWNTs in the form of BPs. They found a linear dependence of the electrical resistance on strain. A dense array of CNTs was expected to exhibit higher sensitivity to local

distributions of stress and strains in the host material. The BPs had the ability to sense stresses and strains in different directions due to the isotropic structure of the film. The currently difficult issue of the quality of the CNTs dispersion, which affected the electromechanical properties of the nanocomposites and may be detrimental to form a robust conductive nanotube network, was avoided [40].

Rein et al. [40] embedded BPs in polymers with different elastic properties and the electrical resistance turned out to change similarly for all polymers. In the highly ductile polymers, the resistance changes of the BP sensors could be measured for strain higher than 30%, which indicted the high sensitivity at large deformation. They also demonstrated BPs sensors were sensitive to the local defects, which was to say that the BPs sensors were highly sensitive to local distributions of strain and stress with the capability to sense those in different directions.

Dumee et al. [63] reported that the BP membrane they fabricated exhibited a high contact angle (113°), high porosity (90%), and a relatively low thermal conductivity of 2.7 Kw/m2h. Based on those properties, the self-supporting CNT BP membranes could be used for desalination in a direct contact membrane distillation. As a proof of concept, the performance of BP could be better than the conventional polymeric membranes.

Vohrer et al. [49] applied BPs as electromechanical actuators, also called “artificial muscles”, which was important application for robotics. It was the

first time to analyze forces and displacements vertical to the BPs planes. Among different prepared CNTs, the BPs made from high-purified CNTs show the best actuation performance. The fastest observed actuation time was about three seconds with the thickness of 35 μ m. It showed a clear voltage dependency of the actuation amplitude within a certain region.

Recently, BPs/polymer nanocomposites have received high recognition in various applications, such as water filters, temperature sensing, strain sensing, fuel cell electrodes, coating, electrical applications such as electrostatic dissipation, electrostatic painting and EMI shielding [34], substrates for never cell growth, and artificial muscles [46, 50-54, 64, 65].

The system was reported to behave as a reversibly flocculated dispersion. The structure of the dispersions was highly sensitive to the strain in the linear viscoelastic region (LVR) extending to strains of 1% [45]. The viscosity, storage modulus and the loss modulus were found to increase, which could be explained by the high aspect ratio of CNTs and high surface area [66]. To be more specific, the increase in viscosity associated with the addition of CNTs was more significant than the cases with CNFs and carbon black. It is known that the agglomerates of the fillers may cause higher viscosity [67], and the nanocomposites with poorly dispersed CNTs have been reported to exhibit higher storage modulus and loss modulus, which all indicated that the poor dispersion can reduce the mechanical properties of the composites. On the other

hand, the well-dispersed CNTs showed increases in electrical and thermal conductivity, and a low percolation threshold [44].

Improved dispersion of CNTs is one of the key issues in CNTs/polymer composites fabrication and applications [68].

Above all, the uniform dispersion is critical for the mechanical electrical and thermal properties of BPs and BPs-based nanocomposites.

1.4 Introduction of BPs fabrication

As mentioned in 1.3, dispersion of the CNTs in polymers has been the difficulty for the development of advanced nanocomposites. The larger specific surface area, the larger aggregates, the harder to disperse.

SWNTs have the largest aspect ratio while the MWNTs exhibit a much smaller one. However, that also makes MWNTs easier to disperse because lower specific surface area provides lower attractive forces between CNTs themselves. Since the sufficient interfacial bonding is desired for stress transfer, and MWNTs provide a smaller interface and lower aspect ratio, which means only the outermost layers get involved. The MWNTs are bundled together by Van der Waals forces, and generally entangled in the form of curved agglomerates while the SWNTs are produced as bundles. According to the references [4, 44], the dispersion state of CNTs may influence the storage modulus, viscosity, electrical conductivity. Therefore, from the mechanical properties reinforcement only, SWNTs and DWNTs have better potential over MWNTs.

However, from the perspective of tunneling resistance, the lager the tube diameter is, the lower the tunneling resistance turns to be. Based on these properties, MWNTs are the better candidate for the electrical applications in this work. The thermal energy alone is not enough to break the potential energy barrier to aggregation. The electrostatic charging of CNTs can be employed to aid the dispersion and hinder the aggregation.

There are two common approaches to achieve the uniform dispersion: mechanical methods and chemical methods [69]. For mechanical methods, it usually refers to ultra-sonicating, milling and shear mixing. There are two short comings, one is CNTs may not break down completely and the other is it can shorter and thinner the CNTs due to the mechanical force. For chemical methods [70], it means surfactant or chemical functionalization may be used to the surface of the CNTs. Acid treatment using vapor nitric acid (HNO_3) [71], liquid HNO_3 [72, 73], or the mixture of HNO_3 and sulfuric acid (H_2SO_4), oxygen (O_2) plasma processes [43, 74-76], and oxidation using $KMnO_4$ [73], H_2O_2 [6, 73] thermal heating under air [77], or UV-ozonolysis [77] are commonly used to introduce covalent bonds to the CNTs surface, while surfactants like Triton X-100 is commonly used to introduce non-covalent bonds. It is found that the functionalized CNTs possessed better dispersion but apparent increases of surface defects of CNTs were commonly revealed by Raman spectra, which indicates that the functionalization would weaken the interfacial bonding between graphene sheets of the CNTs and the transfer

efficiency of applied load could also be reduced [44]. It is reported that the functionalized CNTs can achieve a better homogeneous dispersion into the polymer by improving the interfacial adhesion of CNTs/polymer composites, with the cost of considerably damage to CNTs resulting in both mechanical and electrical properties [46, 78].

The most common method used by many researchers to fabricate BP membranes is the vacuum filtration approach [40, 48, 49, 58, 79-81], as shown in Figure 1.2.

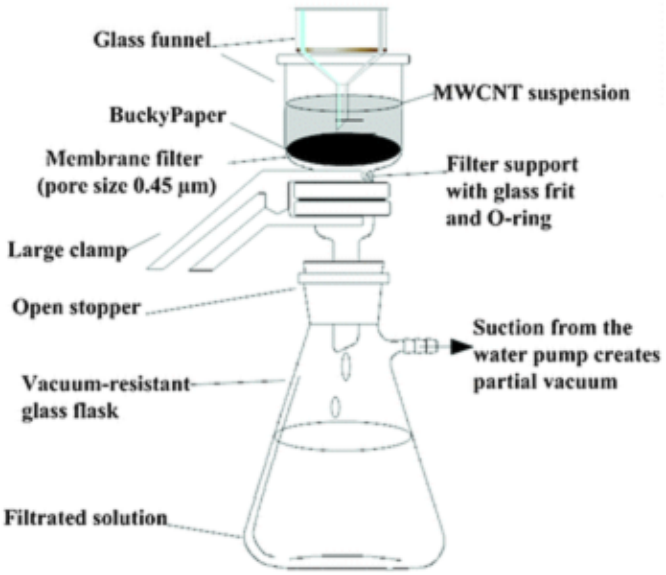

Figure 1.2: Vacuum filtration to fabricate BP membranes [48]

In this method, the non-ionic surfactant Triton X-100 is widely used. To obtain uniform dispersion during filtration and flexibility, chemical functionalization, like UV/ozone treatment and carboxylic acid-bound functionalization, are applied to assist the better dispersion of CNTs and high performance of nanocomposites.

Generally, to fabricate BPs and related composites, CNTs are dispersed in solvent, such as dimethyl foranmide (DMF) [40, 78, 82] or ethyl alcohol [82]. During the dispersion, surfactant like Sodium dodecylsulphate (SDS) [43, 49] is needed. The non-ionic surfactant Triton X-100 is widely used. To obtain uniform dispersion during filtration and flexibility, chemical functionalization of CNTs could be applied to assist the high performance of BPs [37, 83]. UV/ozone treatment and carboxylic acid-bound functionalization can be used to modify CNTs to improve the dispersion.

After dispersion, the CNT suspension solution where the volume decided the thickness, is filtrated using a glass funnel with various diameters to form different sizes of BPs assisted by vacuum, using a filter like polytetrafluoroethylene (PTFE) [41], a filter paper like P8 filter paper [78] or a nylon filtration membrane [40] with submicron-sized pores, e.g. 0.2 μm [63], 0.4 μm [43, 49], 0.45 μm [40, 82], then washed with deionized water to remove surfactant. The CNTs-based membrane is then deposited on the filter surface and can be peeled off after drying [84]. This method is mature and widely used but there are some disadvantages.

Firstly, this method requires surfactants or chemical functionalization of CNTs to assist the stable homogeneous dispersion. Polyoxyethylene t-octylphenol (Triton X-100) has been reported as the most effective surfactant compared to sodium dodecylbenzene sulfonated (NaDDBS) and Sodium Dodecyl Sulfate (SDS) [69]. Following the filtration, the surfactants turn to be

difficult to remove, which significantly hamper the quality of BP membranes. As for the chemical functionalization, it degrades the intrinsic functionality of BPs for the further applications.

Secondly, the procedure is complicated since it requires sufficient support of equipment and skillful operation. It requires large volumes of CNTs suspension taking several hours, which is considered as time-consuming. During the long filtration, maintaining uniform dispersion is particularly difficult, and also because of the limits of sizes of filters, the vacuum filtration method is not suitable for large-scale manufacture [84].

Last but not least, the functionalization of CNTs is confirmed extensively changes the surfaces of the tubes and the oxygen content increased significantly, analyzed by SEM and XPS [43]. Since the change of sp^2-bonds to nearly sp^3-carbon bonds is expected to alter the electrical properties, the electrical properties may be negatively affected.

Up to now, the vacuum filtration can't achieve the expected mechanical and electrical properties of CNTs. The main reason may due to the low stress transformation between tubes. It is reported that the mechanical properties of BPs mainly depend on the connection between tubes, which is Van der Waals force.

The other method called "Domino Pushing" introduced by Wang et al. [42] was demonstrated to effectively prepare the high quality BP membranes, as shown in Figure 1.3. In their work, MWNTs were prepared by chemical

vapor deposition (CVD) method in lab. In this way, The CNTs were aligned as arrays as it grew on the silicon substrate. In this way, when the cylinder, covered by a microporous membrane, pushed the CNTs, all CNTs in the CNT array could be forced down to one direction and attracted together due to the strong Van der Waals force. In this method, no surfactant was used. BPs possessed the advantages as being flexible, higher density, and high thermal and electrical conductivity.

But in these methods the fabrication method was complicated, time-consuming where the MWNTs used were produced in lab instead of purchasing, which added a lot of extra work before the fabrication of BPs. It had the difficulty with the purification of the surfactants. What's more, there was another factor to mention. The chemical functionalization could improve the adhesion bonding between CNTs and epoxy, which contributed to the improvement in mechanical properties to a certain extent. However, when it came to the electrical applications, the sp^2-carbon-bonds would be changed to nearly sp^3-carbon-bonds, which resulted in negatively effect of the electrical properties [53]. The conclusion can be drawn as the chemical functionalization of CNTs is not an ideal method for electrical applications.

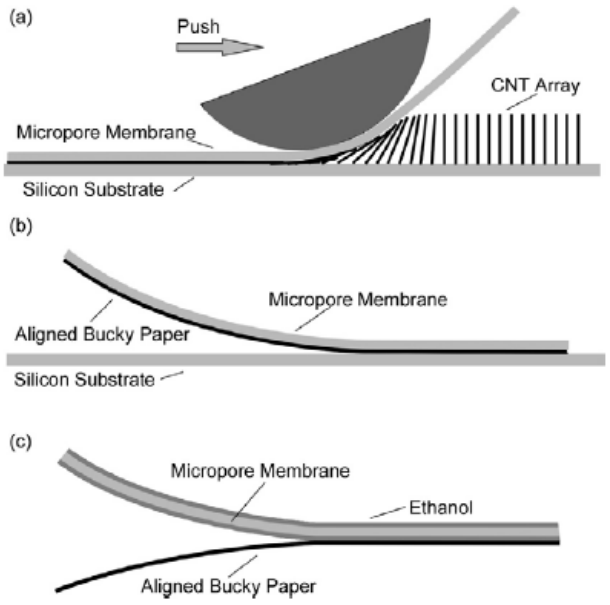

Figure 1.3: "Domino Pushing" method to fabricate BP membranes [53]

It is reported that BPs with diameter ≈ 78mm and thickness 30 - 40μm dimension is the lowest thickness that still enable peeling off without deformation or destruction [43].

1.5 Thesis objectives and structure

In this thesis an easy and novel fabrication approach is reported. The developed method does not require any surfactant in the fabrication process, therefore the nanoparticles are not polluted by any chemicals. Besides the conventional neat MWNTs-based BPs, new hybrid BPs based on Graphene (GN) and MWNTs have been fabricated and the ratio of MWNTs/GN can be changed to get different structures and properties. The BP membranes are obtained, and nanocomposites are developed for sensing applications. The BPs/epoxy nanocomposites were fabricated and tested for the various properties such as microstructure, structural homogeneity and electrical

conductivity [85, 86]. The electrical conductivity indicates BPs can be embedded in the epoxy composites and applied for strain sensing. As shown in Figure 1.4, the objectives and structure of this thesis is summarized.

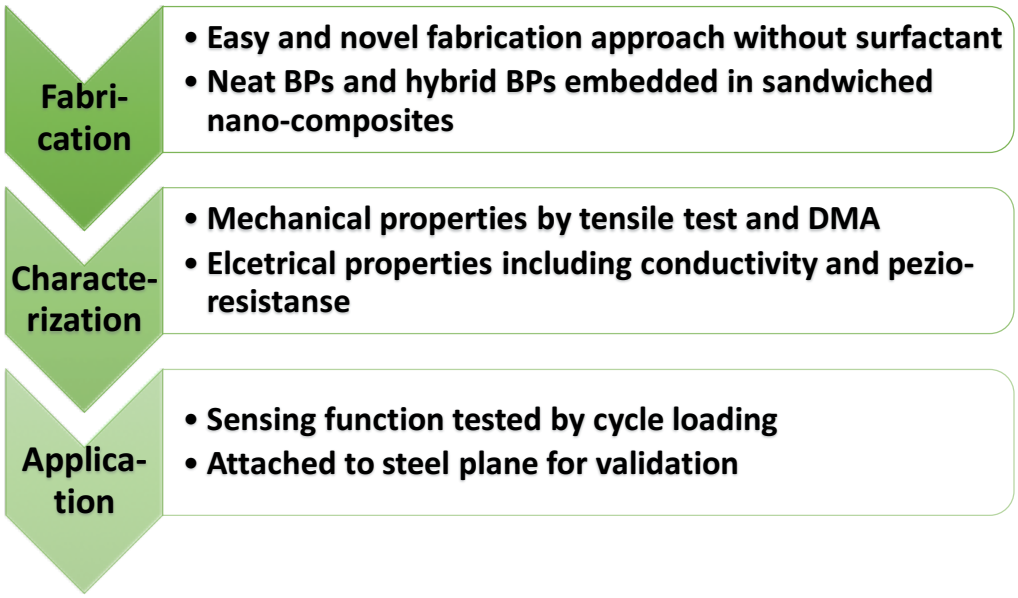

Figure 1.4: Thesis objectives and structure

Chapter 2:

Fabrication of BPs and BPs embedded nanocomposites

Introduction

In this chapter, the detailed fabrication processes for BPs and the BPs embedded composites are demonstrated.

There were two main types of BPs fabricated, neat CNTs-based BPs and hybrid BPs made from CNTs and GN. The neat CNTs-based BPs can be formed as a shape of sheet but the neat GN can't be formed into an intact sheet. Based on this phenomenon, CNTs and GN were mixed at different ratios to fabricate hybrid BPs. A set of experiments was carried out to find the threshold ratio of CNTs versus GN for hybrid BPs fabrication.

The nanocomposites were made by coating BPs with epoxy. The copper wires were attached to BPs with silver paint and embedded in epoxy for the further electrical tests. Because of the frigidity of BPs, coating BPs with epoxy can protect the sensors. Besides, the bulk of the epoxy specimen contributes to achieving a homogenous deformation alone BPs.

2.1 Fabrication process of the BPs

In this work all of the following listed materials and reagents were used as received. The MWNTs employed in this work were supplied by US Research Nanomaterials, Inc. (Product No. US4400). GNs were supplied by Cheaptubes. The solvent used was methanol purchased from Sigma Aldrich. The epoxy

system was supplied by Fiber Glast Inc. (Product No. 2120 Epoxy Resin & Harnder).

Note that no surfactant involved during the fabrication in order to avoid contamination to CNTs which would result in reduced electrical properties and blocking the contacts [87] between particles including MWNTs and GN.

Two types of membranes were fabricated. The first type of membranes consisted of the pristine MWNTs, called neat BPs, while the other type of membranes was the hybrid membranes based on the mixtures of MWNTs and GN, called hybrid BPs. The fabrication procedures of these two types of membranes were similar.

To make it clear, the fabrication of neat BPs was demonstrated first. The membranes fabrication method was based on the MWNTs dispersion in a solvent followed by slowly applying the proper pressure to form a thin membrane, as shown in Figure 2.1.

200 mg MWNTs were stirred in 40ml methanol solvent, followed by tip-sonication for 2 h. Upon completion of the dispersion process, the solution was evaporated in water bath till the high-density slurry was obtained. The slurry was spread onto a porous circular Nylon filtration film on the top of a plastic film. The slurry was slowly pressed until the compression force reached up to 20 tons. The freestanding membranes were peeled gently off the Nylon film after the drying process was complete. The detailed fabrication process was shown in Figure 2.1.

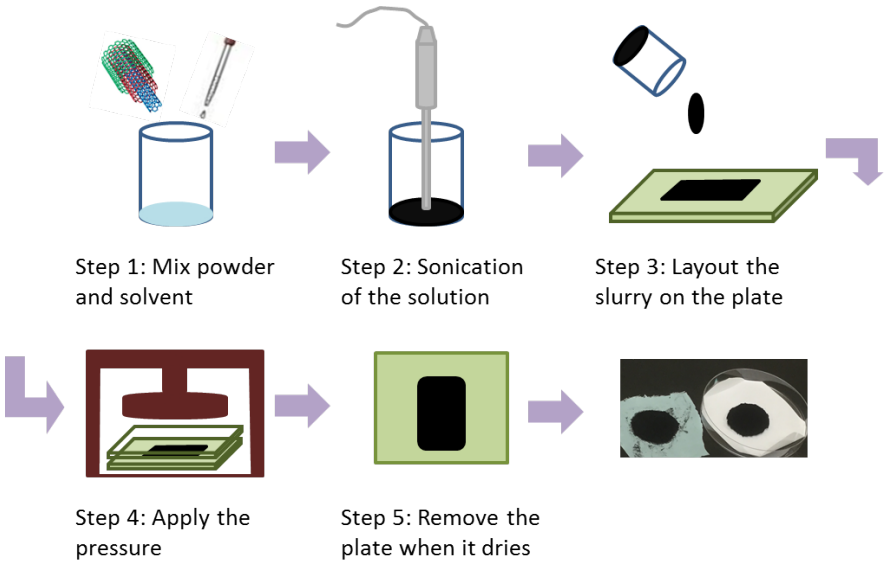

Figure 2.1: Fabrication process of BP membranes

MWNTs and methanol solvent were stirred by hand. To select the type of solvent, there are two factors to be considered. One is the intermolecular forces between the solvent and MWNTs. The affinity is strong and helps with the solubility [88, 89]. The other one is that the solvent is supposed to be easy to remove. MWNTs are soluble in methanol, and the methanol has a low boiling point and easy to evaporate.

Longer sonication time helps break nanotube aggregation but intensive sonication also ends up in breaking the CNTs into segments. It is reported that after 100 minutes the bundles obviously shorten while after 200 minutes the length of CNTs significantly decreases. It has been observed that 10 to 100-minute sonication would help break the aggregation effectively, and after 100 minutes the bundle size doesn't change much but the length keeps decreasing

[69]. Therefore, sufficient but proper sonication is crucial to have dispersion without too much segmenting the CNTs length.

In this work the tip-sonication for 2 h method was employed to break the Van der Waals force among the particles and achieve the homogenous dispersion. Only in this way, a uniform sheet of BP could be expected. Besides, the ultra-sonication could lead to the evaporation of methanol solvent.

After the sonication, a 2 h water-bath evaporation was applied to remove the extra methanol solvent, until a highly viscous slurry of MWNTs with methanol was obtained.

The slurry was laid up on the Nylon membrane under which with a filter paper, and they were put on the aluminum plate which was covered by a plastic sheet. The plastic sheet was used to avoid adhesion between BPs and compression plates, and protect the compression plates from the methanol solvent. The filter paper was used to absorb extra methanol solvent and the Nylon membrane was porous, which helped methanol solvent to flow out into the filter paper gently instead of crashing out rapidly and causing cracks within BPs.

The hydraulic press was used to compress the slurry into a thin uniform membrane. 20-ton force was applied. This process had to be slow because the methanol needed to be removed slowly and gently or the path of methanol solvent gushing out would be left which would be random cracks in BP membranes.

At last, BP membranes with the plates were placed at the room temperature for 24 hours to dry. The intact sheet of BP could be peeled off after drying and removing the plates.

The fabrication procedure of hybrid BPs was similar to the neat BPs. The differences were mainly in the powder mixture. The hybrid BPs were based on the mixtures of MWNTs and GN at different weight ratios.

In Figure 2.2, the main equipment in the fabrication process was shown. They were the tip sonication for dispersion, magnetic stir for water bath evaporation, plates and membranes for lay-up and the hydraulic press for applying the pressure.

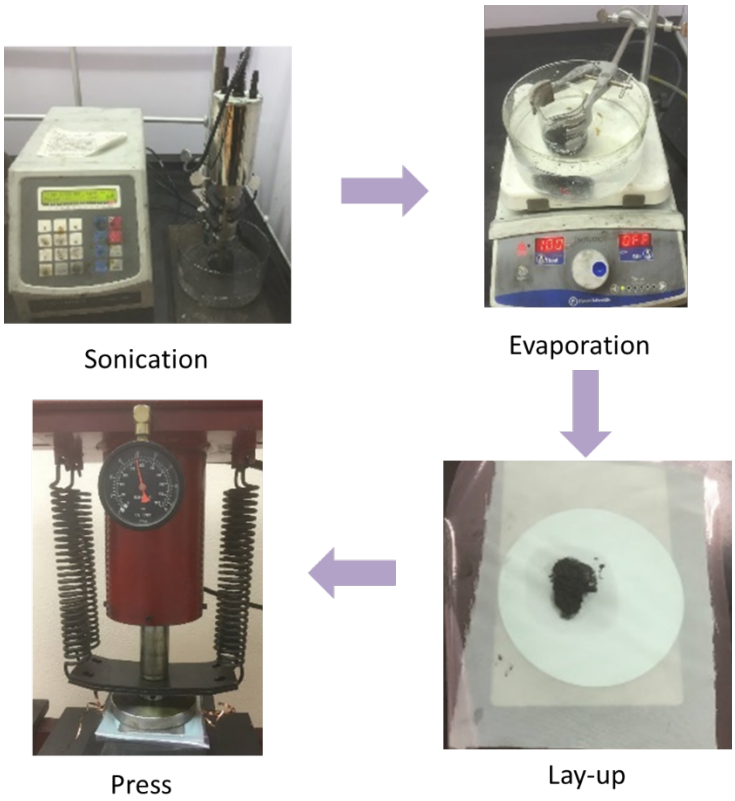

Figure 2.2: The main equipment in the fabrication process

The typical membranes prepared as neat BPs and hybrid BPs were shown in Figure 2.3. For 125mg MWNTs, a round BP with 3.5 cm diameter could be obtained. For 140mg MWNTs, the diameter could increase to 5 cm. Figure 2.3 (a) showed the image of a round neat BP, and (b) showed the image of a round hybrid BP.

BPs fabricated by this method without chemical functionalization were brittle and easy to break. This may due to the MWNTs were connected by the Van der Waals force, which is less than 1% of Young's modulus of a single CNT. To imporve this, strong acid can be applied to add carboxylation, which can add functional groups to the CNTs surfaces and imporve the fracture toughness property on a macro level. In the case of this work, epoxy coating was employed to protect BPs.

(a) 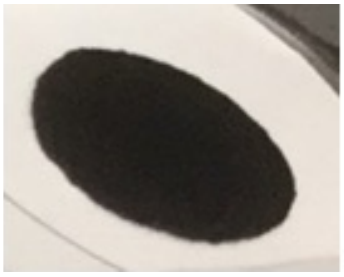 (b) 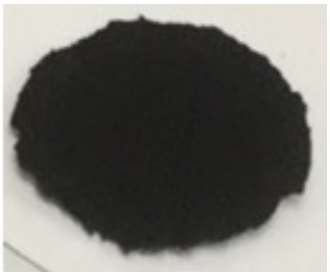

Figure 2.3: (a) Image of a round neat BP, (b) image of a round hybrid BP

There are two basic requirements for a sheet of intact BP: i) from the macro scale, the morphology is expected to be an intact sheet instead of a bundle of powders and there are no cracks in the sheet (small and uniform rope size distribution [69]); ii) from the micro scale, MWNTs should be uniformly oriented without apparent aggregates (formation of even nanotube networks

[69]). Figure 2.4 (a) showed a failed MWNTs-based BP. Technically, it was not an intact sheet of BP because there were powders remained and random cracks. This failure was due to the poor sonication and the high speed applied when pressed. Figure 4 (b) and (c) showed the failed attempt to fabricate a neat GN-based BP. That was because pristine GN was almost impossible to form a sheet without modification or surfactant in the solvent because GN powders were not dispersible or stable [81].

(a)  (b)  (c) 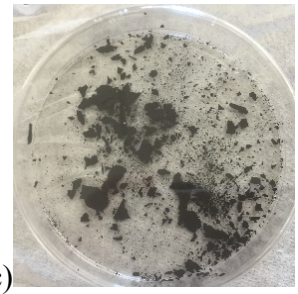

Figure 2.4: Unsuccessfully fabricated BP samples: (a) MWNTs-based BP; (b) and (c) GN debris

Since the sheet can't be formed using pristine GN, while the sheet can be formed using pristine CNTs, there is expected to be a ratio threshold for hybrid BPs. A set of experiments was carried out and the results showed that when the weight ratio of CNTs/GN was 1:5, no intact sheet could be formed and there were only several small pieces could be peeled off, as shown in Figure 2.5 (b); when the weight ratio was 1:6, no intact sheet could be formed, and only small pieces in powder form could be found, which couldn't even be peeled off the nylon membrane, as shown in Figure 2.5 (c). When the weight ratio was 1:4, it could be formed into a sheet but it got much smaller as the GN ratio increased

to 80%, as shown in Figure 2.5 (a). MWNTs/GN = 1:3 started to have cracks at the edge. Then we drew the conclusion that the weight ratio of MWNTs/GN is not supposed to go beyond 1:3. For the future electrical and mechanical tests, hybrid BPs mainly fabricated were with the MWNTs/GN weight ratios as 1:1, 1:2, and 2:1.

(a) 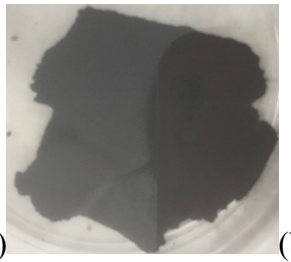 (b)  (c) 

Figure 2.5: Hybrid BPs with CNT/GN weight ratio (a)1:4, (b)1:5, (c)1:6

2.2 Fabrication of BPs embedded nanocomposites

It was reported that the structural properties of functionalized and non-functionalized MWNTs were similar, and the small differences in structural defects obtained in the Raman spectra did not affect the intrinsic conductivity of the two types of CNTs. So it was not necessary to involve functionality to test the electrical conductivity. Samples with values of concentration higher than 4% have been rarely made due to the difficulties associated to the high viscosity and dispersion procedure.

The sensor incorporation with the bulk of the epoxy specimen could help achieve a homogeneous deformation in BP films under tensile test [78, 90] and provide protection to the sensor and electrodes during the mechanical deformation.

Nanocomposite thin films using the BP membranes prepared in last section were prepared. Either neat BP membranes or hybrid BP membranes were used as the inner layer in the nanocomposite thin films. Small rectangles (40 mm × 5 mm) were prepared. Two and four copper wires were attached with silver paint respectively to the membranes' surface as the electrodes and embedded within the nanocomposite thin films for later two and four-probe electrical tests.

The epoxy resin was smeared uniformly on the nylon membranes and BPs. BPs were placed in the center of two smeared Nylon membrane to fabricate the coating structure. The epoxy resin and the cure agent were cured by the stoichiometric ratio at room temperature for 48 h. Figure 2.6 showed the structure of the BPs/epoxy nanocomposites.

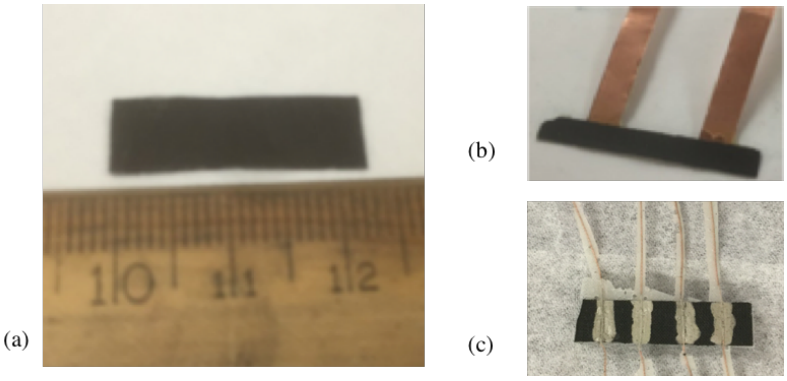

Figure 2.6: (a) Nanocomposite structured with epoxy coat and BP core, (b) and (c) composites with two and four wires for electrical characterization, respectively

The coating material epoxy showed good environment stability. It formed good protecting layers on the conductive BPs core. The nanocomposites could keep the structure and its dimensional stability for a long time in methanol solvent. The sheet of the BP was soon broken down into the powders under

stirring or ultra-sonication treatment. As shown in Figure 2.7 (a), if the BPs were the neat BPs, it would break down into neat MWNTs while if the BPs were the hybrid BPs, it would break down into the mixtures of MWNTs and GN. Compared to BPs, the films exhibited super high dimension stability by keeping its integrity even after 2h sonication, as shown in Figure 2.7 (b). This proved the protection effect of the epoxy resin coating layers.

(a)  (b) 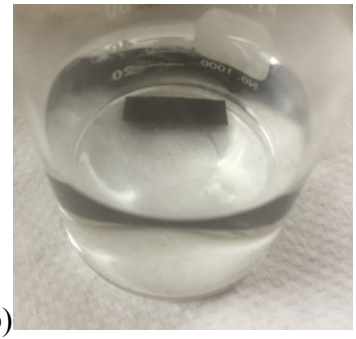

Figure 2.7: (a) The neat BPs broke down during sonication, and (b) epoxy coating protected BPs by keeping its integrity after two-hour sonication

Chapter 3:

Characterization of BPs and BPs embedded nanocomposites

Introduction

In this chapter, the characterization methods and results of BPs and nanocomposites were demonstrated.

The morphologies of BP membranes were characterized using the scanning electron microscope (SEM) in order to investigate the surface fine structure and apparent pore size distributions. The dynamic mechanical properties were characterized by the TA Instruments Q800 Dynamic Mechanical Analyzer (DMA). The mechanical properties were tested by tensile tests using the Micro Mechanical Testing Stage. The max load capacity of this stage is up to 200 N with the force resolution of 0.2 N. The electrical resistance was measured by multi-meter. The electrical resistance measurements of BP/epoxy samples were made using both two-point contact probe and four-point contact probe methods, and the later one was used to eliminate the effect of lead resistance. The change in the resistance of the nanocomposite sample was measured as the response to the strain applied to the tensile specimen.

The detailed comparison of two-probe and four-probe method was addressed. In addition, the scenarios where four-probe method could perform better were analyzed.

3.1 Characterization of BPs

3.1.1 Morphologies of BP membranes by SEM

SEM is a widely used method to investigate structural features of BPs [91]. SEM is an electron microscope that provides surface images of the specimen with a focused beam of electrons scanning across the surface of the sample. A signal containing the surface information is generated and detected at each point along the scan. SEM is not a direct imaging technique but a probe/signal mapping technique. SEM is capable of backscattered imaging for the compositional contrast; secondary electron imaging for surface topography, morphology and particle sizes; Transmitted electron imaging for internal ultrastructure; energy-dispersive X-ray spectroscopy for elemental composition, mapping and line-scans; and electron backscattered electron diffraction for crystallographic information.

Samples for SEM need not to be thin, but must be conducting or semi-conducting and have an electrical path to ground. From this perspective, BPs are the proper specimens because of the electrical conductivity. Since the topography of the BPs is concerned, the secondary electron imaging model is chosen for the imaging.

In this work, the morphologies of BP membranes were characterized using SEM (Zeiss Neon 40 EsB) as shown in Figure 3.1, in order to investigate the surface fine structure and apparent pore size distributions. The resolution of this microscope can reach up to 1.1 nm with dual beam SEM (0.1-30 kV Schottky

emitter) / FIB (2-30 kV Ga liquid metal ion source). An accelerating voltage of 5 kV and a working distance of 2.4 mm were chosen to produce the micro-morphological images.

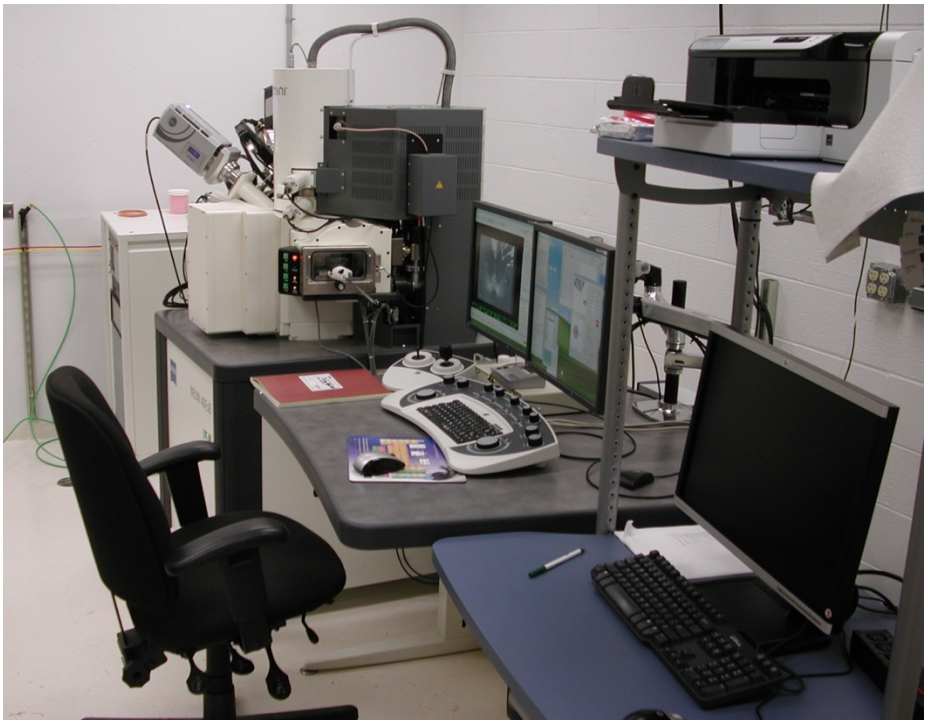

Figure 3.1: SEM for BPs nanostructure characterization

The micrographs of the GN powders, neat BPs and hybrid BPs imaged by SEM were shown in Figure 3.2. A pore was defined as the void between the crisscrossing of particles, meaning CNT-CNT, CNT-GN and GN-GN. There were no macro-pores observed.

Figure 3.2 (a) and (b) showed the surface of a sheet of neat BP which was fabricated following the experimental procedure reported in chapter 2. Figure 3.2 (c) and (d) showed the microstructure of GN powders. Figure 3.2 (e - h) showed the surface of the hybrid BPs.

Figures 3.2 (a) and (b) showed that MWNTs were homogeneously dispersed in the BP films, without visible agglomerates, indicating good tube dispersion and reconnection in the suspension. Figures 3.2 (e) and (f) showed the hybrid BP with 1:1 MWNTs/GN, and Figures 3.2 (g) and (h) showed the hybrid BP with 1:2 MWNTs/GN. The images showed that the tube networks were composed of continuous MWNTs ropes, which were the result of tube self-assembly by Van der Waals force during the pressure. The neat and hybrid BPs were both highly porous. Compare Figures 3.2 (e) and (g), the volume fraction of the 1:2 MWNTs/GN hybrid BP was higher than 1:1 MWNTs/GN hybrid BP, which was because the GN filled the pores of the MWNTs and increased the volume fraction.

In Figure 3.2 (a), MWNTs showed clear definition of each tube and were well dispersed without aggregates. In Figures 3.2 (c) and (d), GN powders showed the spherical shape in micro-scale. In Figure 3.2 (d), in the macro scale, the GN powders showed the GN nanoplatelets possessed stratified structure with small flakes. Those pictures also matched with the results of other researches [92]. Compare Figure 3.2 (e) with (g), since the portion of GN increased, more GN flakes could be seen. What's more, in Figure 3.2 (g), MWNTs enwound GN flakes up and formed a more compact and homogenous nano-structure.

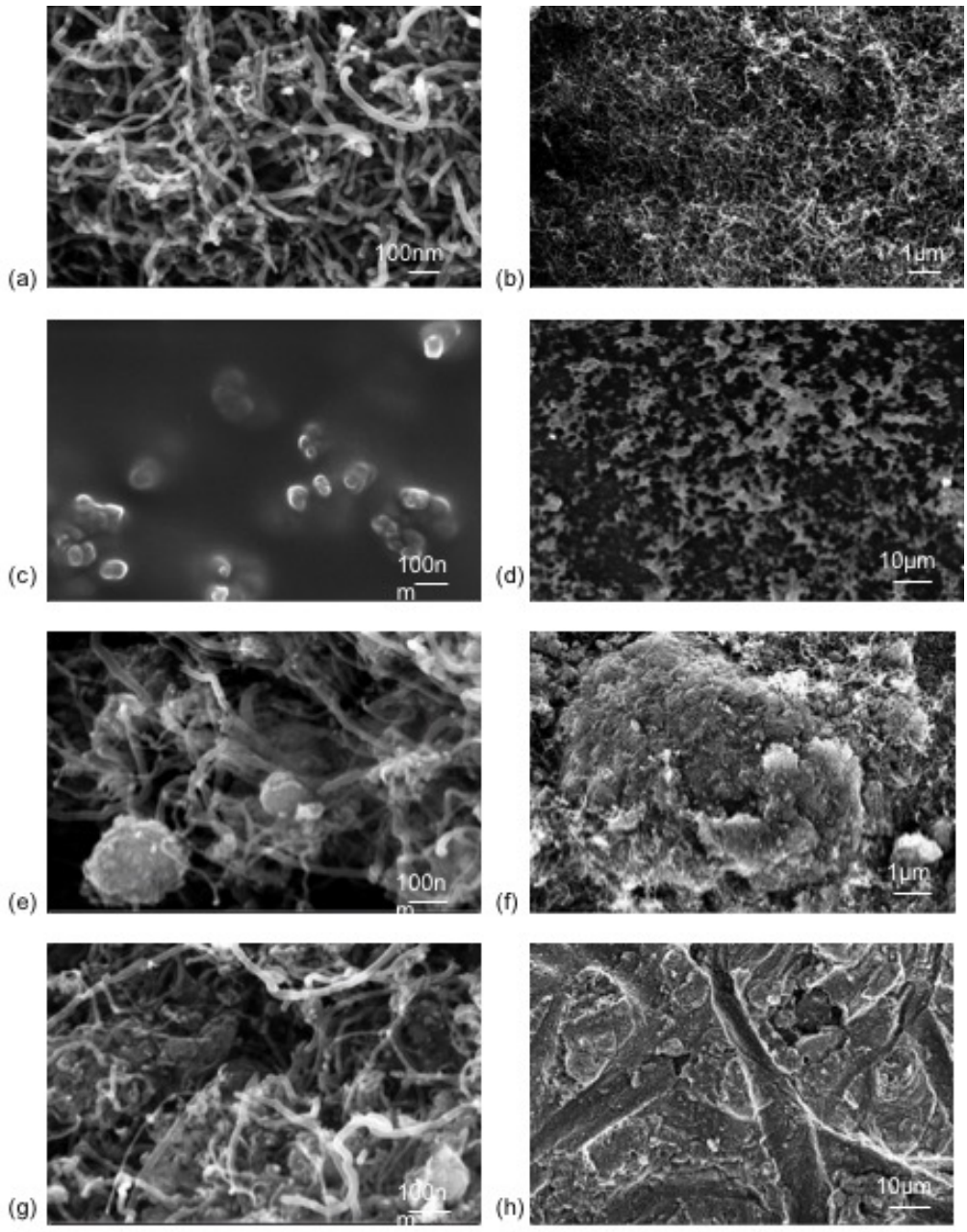

Figure 3.2: (a and b) SEM images of neat BP, high and low magnification, respectively, (c and d) SEM images of GN powders, high and low magnification, respectively, (e and f) SEM images of 1:1 MWNT/GN hybrid BP, high and low magnification, respectively, and (g and h) SEM images of 1:2 MWNT/GN hybrid BP, high and low magnification, respectively.

3.1.2 Electrical conductivity of BP membranes

The pristine epoxy is electrically insulated. Neat BPs and hybrid BPs all showed high electrical conductivity. Since the pristine epoxy is considered to be isolated, the electrical conductivity of the nanocomposite depends only on the property of BPs. Conclusively, the electrical conductivity of the nanocomposites is the electrical conductivity of the BPs.

The digital multi-meter offers both two-probe and four-probe resistance measurement capabilities. These two techniques are not equally suited for all resistance measurement requirements [93]. It is necessary to choose the proper method for the electrical resistance measurement. Figure 3.3 (a) represents a two-probe resistance test configuration, and Figure 3.3 (b) represents a four-probe resistance test configuration.

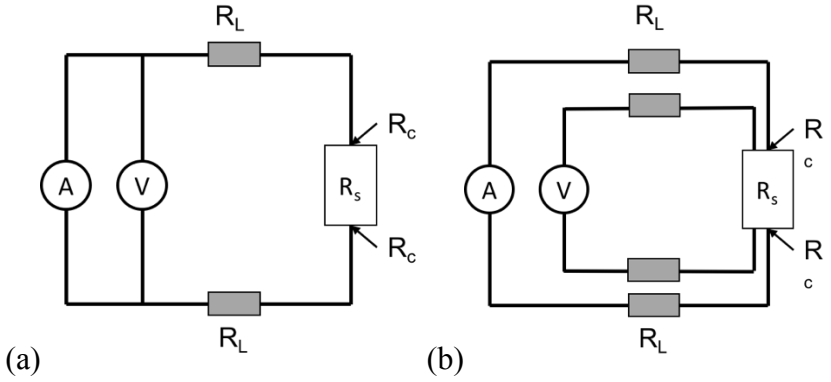

Figure 3.3: Two-probe and Four-probe resistance test configuration

The conventional two-probe method is easier to operate but it may require the calibration with four-probe method during the data processing.

From Ohm's Law: $R_T = V/I = 2R_L + 2R_C + R_S$

where, R_T represents the total resistance, R_L represents the lead resistance, R_C represents the contact resistance, and R_S represents the subject resistance [94].

As shown in Figure 3.3 (a), the test current (I) causes a small voltage drop across the contact and lead resistance. When the subject resistance is small, this voltage drop turns to be significant and is not supposed to be eliminated anymore. The measured voltage (V) can't exactly represent the voltage directly across the subject that we are concerned. The contact and lead resistance become the dominate source of error in addition to the error of instrument. Typically, it is not proper and accurate to use two-probe method when the subject resistance is lower than 100 Ω [95].

Based on the rough benchmarks of electrical resistance of BPs, for a sample with the shape parameters as 20mm×6mm×0.25mm, the resistance is around 100 Ω. Under this circumstance, the measured resistance includes the wire resistance, the contact resistance and the subject resistance. The measured resistance is not accurate enough to accept.

Due to the limitations of the two-probe method, four-probe method is employed to reduce the effect of lead resistance and contact resistance. Four-probe method is also called as Kelvin resistance measurement. The voltage across the subject is measured directly and the small voltage drop through the sensor leads is usually negligible and can generally be ignored for all practical purposes. The measured voltage can be taken as the voltage across the subject resistance. Under this circumstance, the subject resistance value can be much

more accurate than that obtained by two-probe method. It is noted that the voltage-sensing leads are supposed to be connected as close to the subject as possible to avoid the leads resistance [95].

There were two BP samples prepared. Each one is measured by both two-probe method and four-probe method to reveal the influence of lead resistance and contact resistance. As shown in Table 3.1 and Table 3.2, where, L represents Length, W represents Width, T represents Thickness, R represents the mean of measured Resistance, SD represents standard deviation of the measured Resistance, and C represents Electrical Conductivity, the shape parameters, mean and standard deviation of measured resistance, and calculated electrical conductivity are listed to see the differences between the two methods.

Table 3.1: Results of sample 1 obtained from two methods

Methods	L(mm)	W(mm)	T(mm)	R(Ω)	SD(Ω)	C (10^{-3}×Ω×m)
2-Probe	11.01	6.47	0.28	67.35	0.0062	11.0819
4-Probe	11.01	6.47	0.28	65.25	0.0048	10.7336

Table 3.2: Results of sample 2 obtained from two methods.

Methods	L(mm)	W(mm)	T(mm)	R(Ω)	SD(Ω)	C (10^{-3}×Ω×m)
2-Probe	11.19	5.98	0.21	32.14	0.0041	3.6061
4-Probe	11.19	5.98	0.21	29.58	0.00003	3.3189

From the tables above, the electrical conductivity calculated from the measured parameters showed a difference. The electrical conductivity obtained

from two-probe method was larger than the one obtained from four-probe method by around 3 - 8%, where the smaller the resistance was, the larger the error percentage it turned to be, which meant the leads resistance and contact resistance were not supposed to be eliminated in this case, where we wanted to obtain the accurate electrical conductivity. That was to say the four-probe method could get more accurate results for the electrical conductivity of small BP samples.

Compared to the results obtained from two-probe method, the electrical conductivity measured by four-probe method has increased stability with smaller standard deviation. This difference can be explained as the electrical resistance of BP, which is small. The contact resistance is much bigger than that of BP, and the contact resistance plays the main role in the measured resistance. The presence indicated that the four-probe method is the proper way to measure the electrical conductivity accurately.

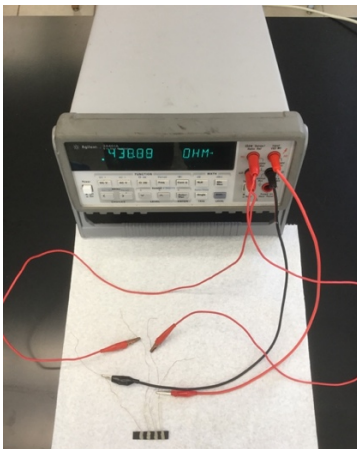

Figure 3.4: Experimental setup for electrical resistance measurement

The electrical conductivity was measured at room temperature using a four-probe method. Figure 3.4 showed the setup for the electrical resistance measurement. The shape parameters were measured using a micrometer gauge (resolution 0.01 mm). There were six types of BPs made, as neat BPs, hybrid BPs with MWNTs/GN ratio as 1:1, 1:2, 2:1, 1:3, 3:1. The shape parameters, mean and standard deviation of measured resistance, and calculated electrical conductivity were listed in Table 3, where, L represents Length, W represents Width, T represents Thickness, R represents the mean of measured Resistance, SD represents standard deviation of the measured Resistance, and σ represents Electrical Conductivity.

Table 3.3: Electrical conductivity obtained from four-probe method

Specimens	L(mm)	W(mm)	T(mm)	R(Ω)	SD(Ω)	σ(S/m)
100%CNT	11.19	5.98	0.21	29.58	0.00003	302
75%CNT	8.24	6.82	0.22	28.44	0.0048	182
66%CNT	7.06	7.14	0.23	26.76	0.0095	160
50%CNT	11.01	6.47	0.28	67.35	0.0062	90
33%CNT	6.60	7.52	0.29	33.93	0.0054	89
25%CNT	9.89	6.74	0.29	69.04	0.0080	73

Though the CNTs have two types, semi-conductive or metallic, the experiments showed the BP was metallic in nature at room temperature. The quasi-linear ohmic behavior indicated that the continuous networks were well-maintained in all these samples. The measured electrical conductivity of both

neat BPs and hybrid BPs were stable, the deviation was less than 0.01 Ω compared to the mean resistance as 30 – 60 Ω.

There are two reasons to explain the electrical conductivity of BPs: i) the intrinsic electrical conductivity of the MWNTs and GN; ii) the inner contact resistance between particles [96]. Since the theoretical electrical conductivity of GN is higher than CNTs, if the electrical conductivity of BPs was dominated by the intrinsic electrical conductivity of both CNTs and GN, then with the increase of GN, the electrical conductivity was supposed to increase in the meantime. However, the calculation of the electrical conductivity showed the tendency that with the increase weight ratio of GN, the electrical conductivity decreased. This showed evidence that the resistance of BP could be influenced significantly by the contact resistance including MWNTs-GN contact and the MWNTs-MWNTs tube contact. In the BPs network, the electrical conductance is governed by the inner-tube junctions and exhibits a percolation-type behavior [96].

The pure epoxy resin exhibits the electrical conductivity of 3.3×10^{-15} S/m. According to the reports in other references, the value of the conductivity can be achieved as 4.3×10^{-1} S/m when the MWNT percentage goes up to 1%. Because of the nanotube/nanotube contact resistance, the conductivity doesn't reach the values obtained for dense films. The tunneling resistance was found to play a dominant role in the electrical conductivity in composites and the maximum tunneling distance is about 1.8 nm [38]. What's more, when the layer

thickness increases, the tunneling resistance increases very rapidly. The results indicate that the electrical conduction depends strongly on the content of CNTs, the contact resistance plays a dominant role in the electrical conduction of CNTs-based nanocomposites. At the certain content of CNTs, the contact resistance plays the dominant role in electrical conduction. This can explain that the reported electrical conduction variance may be due to the different CNTs network. Based on these results, we can see the CNTs mats or BPs have relatively smaller contact resistance and results in much higher conductivity. In CNTs mats or BPs, the intrinsic resistance of CNTs can contribute more.
Based on Table 3 and the results observed by other researches, the conclusion can be drawn that the electrical conductivity of BPs is dominated by the inner contact resistance between particles.

On the other hand, there may be another reason for the electrical conductivity decrease, which may contain certain value for further research. Since we purchased GN particles instead of thin oxidized GN sheets, this may result in the resistance of GN not being as ideal as GN sheets reported by other researchers. Due to the high expense of oxidized GN sheets and here we wanted to prove the concept at the stage, the results using oxidized GN sheets may be different from the results we got using larger GN particles. In this work, we want to address the conditions of using two-probe method and four-probe method.

As stated above, the four-probe method is more stable and accurate because the voltage measured between the middle two wires is used to eliminate the effect of leads resistance and contact resistance. This effect is more significant when it comes to the situations where i) the subject resistance is small compared to lead resistance, for example when the subject resistance is under 100 Ω and the lead resistance is above 1 Ω, it is better to use four-probe to measure the resistance since the error will result is more than 1% in addition to that of instrument and operating; ii) the long distance measurement where the long length of leads result in a big increase of leads resistance; iii) semi-conductive material, whose resistance conductivity varies between 10^{-5} - 10^{7} Ω/m in the room temperature and is influenced by temperature and voltage. When it comes to semi-conductive material, four-probe method is required instead of being preferred.

Apart from the three conditions discussed above, two-probe method is acceptable because the error is negligible compared to the measured resistance or when the accurate resistance is less concerned than the resistance change.

Those are the reasons why we used four-probe method to get the accurate resistance while applied two-probe to observe the resistance change because when it came to the characterization of electrical-mechanical properties that cared more about the tendency of resistance change than the accurate conductivity calculated, it was acceptable when we had samples of proper size and the measured resistance beyond 100 Ω. Two-probe method was used to

characterize the electricity change with the deformation used by other researchers [73].

Note that, when measure the resistance regardless of the methods, the voltage-sensing leads are supposed to be connected as close to the resistance under the test as possible to avoid the leads resistance.

3.2 Characterization of BPs

3.2.1 Mechanical properties of nanocomposites

To compare the mechanical enhancement effects of the BPs, nanocomposites with BP core as neat BPs, hybrid BPs with CNTs/GN ratio = 1:1, 1:2, 2:1, 1:3 and 3:1 were prepared.

Tensile test was carried out to characterize the in situ mechanical properties, using the Micro Mechanical Testing Stage from Gatan, as shown in Figure 3.5. The max load capacity of this stage is up to 200 N with the force resolution of 0.2 N.

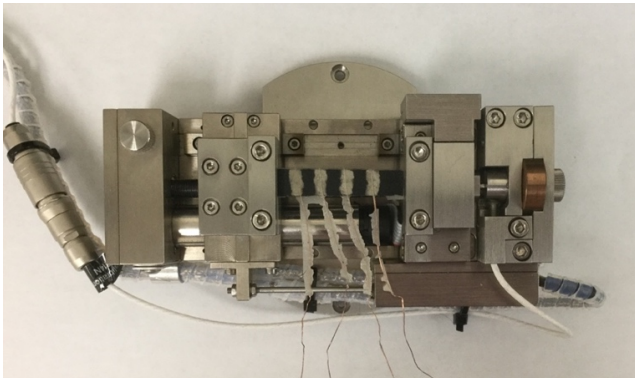

Figure 3.5: Tensile stage for mechanical property characterization

The quasi-static tests were applied to test the failure strain of the sensors at high levels of stresses and strains. From Figure 3.6, the nanocomposite

performed elastic deformation under around 0.1 mm deformation and 20 N force. After that, the nanocomposite started to yield. Since it presented viscoelastic properties, it had both the plastic deformation and viscos deformation until it failed at around 2.6% extension. Due to the viscoelastic properties of the polymer based nanocomposites, the deformation shows the phase lag response to the force.

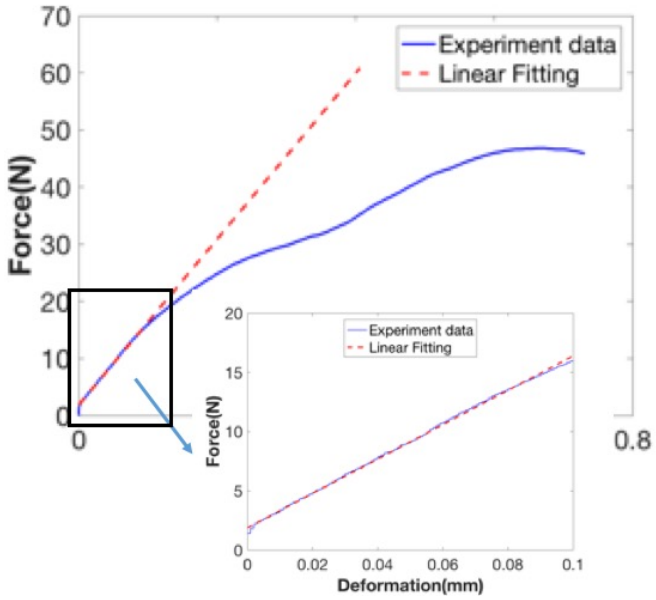

Figure 3.6: Tensile test results revealed the deformation between 0-0.1 mm was the feasible interval

From the results of tensile test, deformation between 0 - 0.1 mm will be the feasible interval, because the cold hardening and cramp can be significantly avoided.

From the perspective of a condensed state, polymer based composites are supposed to be liquid state because the molecular arrangement presents short range-order without long range-order structure. On the other hand, from the

perspective of mechanical state, they are supposed to be solid because they have both shape and bulk. Similar to the glass, polymer and its composites can be considered as bulk with liquid state, which is also called glassy state.

Compared to the conventional solid materials like metal or ceramics, polymer and its composites possess general elastic state. In the meantime, they have the advantage of high elasticity under a certain condition. The unique state is also called rubbery state.

The reason why polymer and its composites have extraordinary elastic state, namely the rubbery state, is due to the deformation mechanism is different from the general elastic material.

The general elastic deformations result from the changes of bond length and bond angles between molecule and/or atom, caused by the stress. The highly elastic deformations result from that the long and soft macromolecular chains extend with the stress from the original random polymer coil.

Based on the experiments by other researchers, the mechanical properties of polymer bulk also showed the dependence of time, which means the temperature ramp, tensile speed, etc. That the elastic properties are dependent on time factors is defined as the elasticity with viscosity of polymer. However, on the other hand, melting the polymer shows elastic deformation when irreversible plastic deformation happens. This reveals that the polymer possess viscosity with elasticity.

From those known facts, the unique mechanical property of polymer and its composites is called viscoelasticity.

As we know from mechanics of materials, the ideal elastic bulk follows Hooke's Law, $\sigma = E\varepsilon$, in which, E is called Young's Modulus representing the stiffness of the material, namely the capacity standing up to the deformation. The ideal viscos liquid follows the Newton's laws $\tau = \eta \frac{d\gamma}{dt}$, in which η is called viscosity, namely stress is proportional to strain rate.

Introduction of the basic concepts of elastomer and viscoid as above, is to demonstrate the mechanical properties of polymer and its composites as following.

The polymer and its composites are neither elastomer nor viscoid. Instead, they are viscoelastic bodies, which means they don't follow either Hooke's Law or the Newton's laws. The behavior of the viscoelastic body is right in the between. The stress depends on both the strain and the strain rate.

When the constant stress is applied, the strain of ideal elastomer doesn't change with time, while the strain of ideal viscoid increases linearly with time. However, when it comes to the viscoelastic body, the strain changes non-linearly with time. When the stress is removed, the stain of ideal elastomer reverts immediately, while the strain of ideal viscoid remains unchanged. However, when it comes to the viscoelastic body, the strain reverts partially and gradually with time. This is because The viscoelastic body possesses both the characteristics of elastomer and viscoid. When the stress is applied, part of the

work of stress is stored as elastic energy, the other part of the work of stress is consumed as heat. When the stress is removed, part of the deformation can revert as elastic deformation, and the rest can't revert as viscous deformation.

Polymer and its composites are classic ones of viscoelastic bodies. Generally, creep, stress relaxation, and the damping under dynamic stress are considered as the most classic in the presences of the viscoelasticity.

To make it clear, creep is the tendency of a solid material to move slowly or deform permanently under the influence of mechanical stresses [97]. More specifically, creep means the strain gradually increases with time under certain temperature and constant stress. stress relaxation is the observed decrease in stress in response to the same amount of strain generated in the structure under certain temperature [98].

Also due to the viscoelastic properties of the polymer based nanocomposites, the deformation shows the phase lag response to the force. When the cycle load tensile test is applied, the nanocomposites show the classic dynamic mechanical properties of viscoelastic polymer-based nanocomposites – Figure 3.7 (a) presents the stress relaxation while Figure 3.7 (b) presents the damp. Figure 3.7 (c) shows that there is elastic deformation, plastic deformation, and viscos deformation, which means that part of the deformation can be reversed, while part of the deformation remains, which results as cold hardening, and part of the work was lost during the viscos deformation.

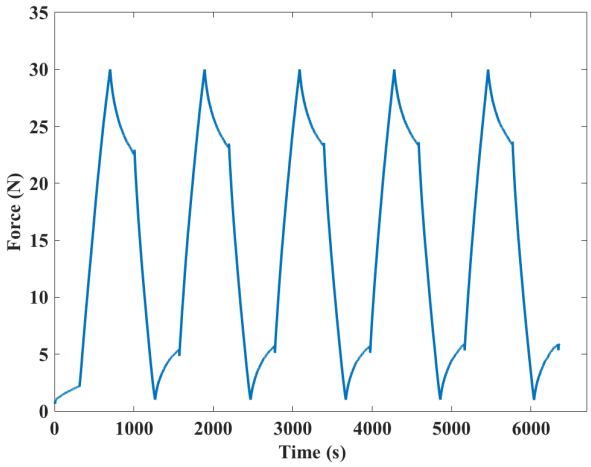

(a)

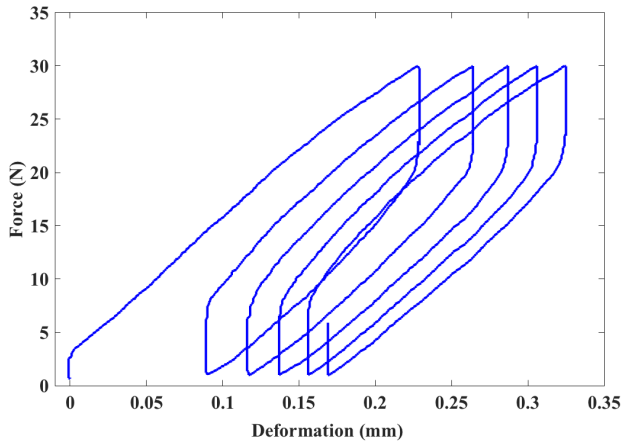

(b)

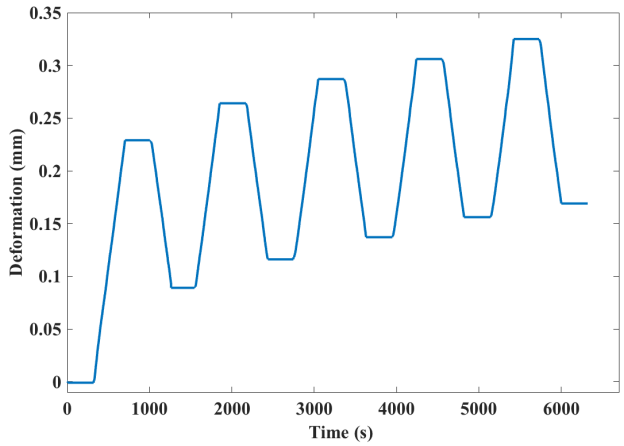

(c)

Figure 3.7: Deformation of nanocomposites due to viscoelasticity

3.2.2 Dynamic mechanical properties of nanocomposites

There are two main types of mechanical properties concerned for composite samples. One is the static mechanical properties, while the other is the dynamic mechanical properties.

The former one refers to the response of samples to the constant or monotone increasing strain or stress, which was introduced and tested in 3.1.3, The latter one refers to the response of samples to the vibration, namely alternating strain or stress.

Dynamic Mechanical Thermal Analysis (DMTA) is a method to monitor and measure the changes in dynamic mechanical properties over a temperature range.

Fatigue is one of the dynamic mechanical properties, which is tested under higher stress. Compared to that, the DMTA test carried out for our samples were under much lower stress. The properties concerned here are dynamic stiffness and damping.

The objectives of DMTA is to find out i) the stiffness and damping of materials under certain conditions like temperature, frequency, strain, stress, atmosphere, and humidity, ii) The changes of stiffness and damping with the changes of temperature, frequency or time.

To measure it, there are two types of bending deformation, one is three-point bending while the other one is cantilever bending. In this work, three-point bending is employed.

The equipment used in this work is the TA Instruments Q800 Dynamic Mechanical Analyzer (DMA), which is a precision thermal analytical instrument designed to test the mechanical properties, specifically viscoelastic properties, such as modulus and damping of rigid and soft solid materials [99]. This instrument is capable of determining changes in properties resulting from changes in seven experimental variables: temperature, time, frequency, stress, force, displacement and strain, of samples which can be in bulk solid, film, fiber, gel, or viscous liquid form. The properties can be obtained from this instruments includes: modulus, damping, creep, stress relaxation, glass transitions, and softening points. The TA Instruments Q800 DMA was shown in Figure 3.8 (a).

In this work, temperature changes, constant frequency, constant applied strain were the required experimental variables. Modulus including storage modulus and loss modulus was the concerned properties.

(a)  (b) 

Figure 3.8: (a) DMA (Q800), (b) three-point bending clamp

There are two main types of clamps that can be classified as either tensioning or non-tensioning clamps. The clamp in this work is the three-point bending clamp, which is one of the tensioning clamps, which means a positive force (preload force) is required to be placed on the sample at all times. The three-point bending clamp, as shown in Figure 3.8 (b), has two basic parts – a movable clamp which is in the middle, and a fixed clamp (also called a stage) which is at the side.

This clamp is used for stiff and low damping samples like metal, ceramics and highly filled thermosetting polymers. Since the nanocomposites have high stiffness and are coated with epoxy which is thermosetting polymer, three-point bending clamp is the proper one to apply for the test.

TA Q800 DMA has multiple operating modes available. Since there are plenty of modes to choose from, a suitable mode for our test is crucial to obtain the parameters that are interested. In the work, temperature and frequency dependence of storage and loss modulus, and tan δ are concerned, so that DMA multi-frequency strain mode was chosen. Under this mode, temperature ramp/ frequency constant was set up.

According to other researchers' work, DMA method has been widely used to measure the glass transition temperature and tell the enhancement of the fillers. In this work, the epoxy was cured at room temperature which made the glass transition temperature pretty low and the improvement of that was not the mean concern here. Under this circumstance, we turned to compare the

enhancement of BPs with different MWNTs concentration to find out the preferable weight ratio of the hybrid BPs. There is one parameter to clarify first. Because there were two types of BPs fabricated, one was the neat BPs, while the other is hybrid BPs with different weight ratio between MWNTs and GN. In order to avoid misunderstanding, here, we defined that the neat BPs as 100% MWNTs BPs, the hybrid BPs with MWNTs/GN ratio 3:1, 2:1, 1:1, 1:2, and 1:3 as 75% MWNTs BPs, 66% MWNTs BPs, 50% MWNTs BPs, 33% MWNTs BPs, and 25% MWNTs BPs, respectively. In the following content, for example, 75% MWNTs is referred as the concentration of MWNTs in the BPs, instead of MWNTs in the epoxy matrix. The DMA testing results were shown in Figure 3.9. Figure 3.9 (a) compared the enhancement of storage modulus between samples at different MWNTs ratios as well as showed how storage modulus changes with temperature. Similarly, Figure 3.9 (b) and (c) compared and showed loss modulus and tanδ, respectively.

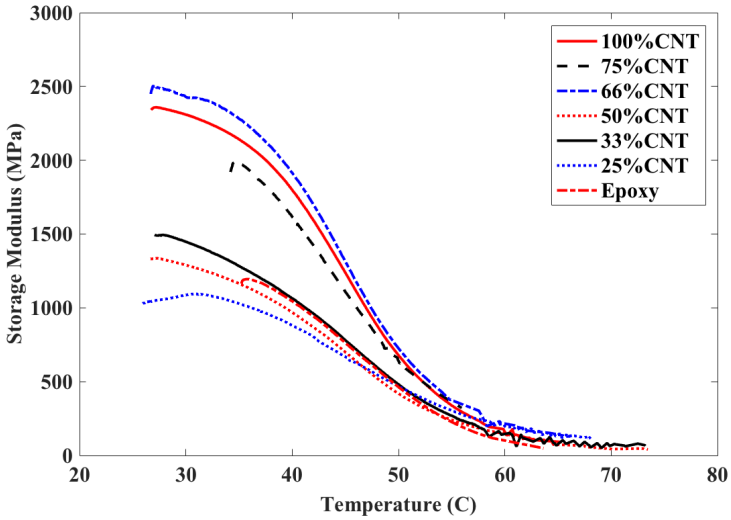

(a)

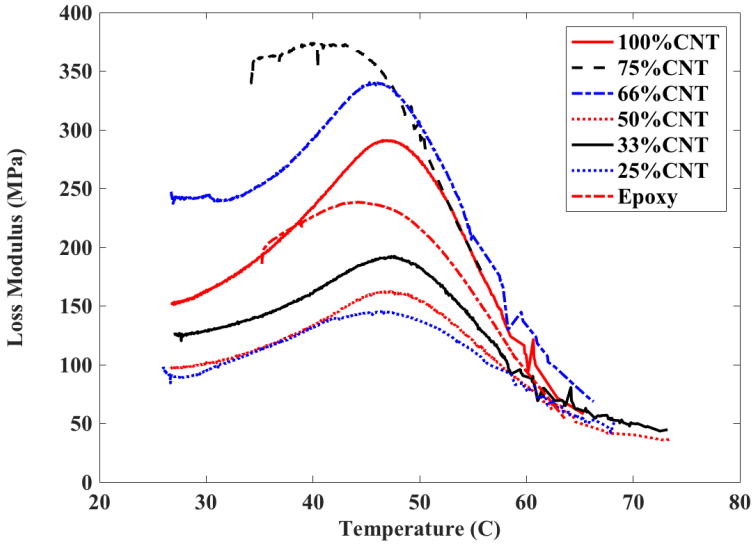

(b)

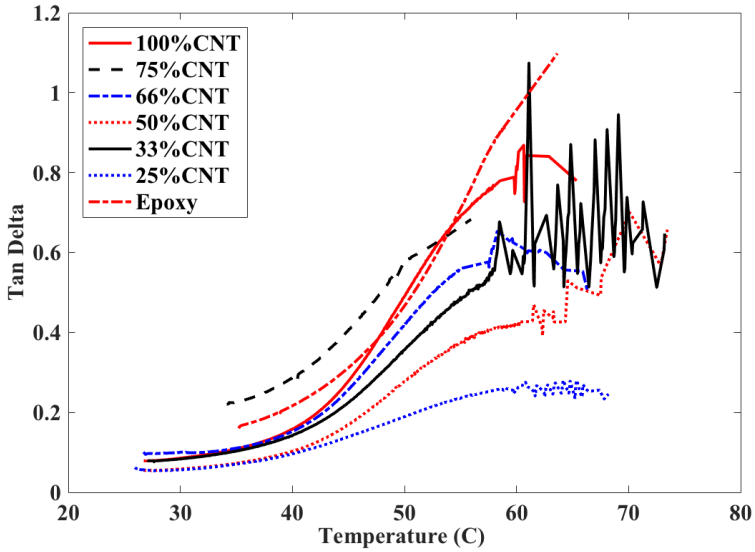

(c)

Figure 3.9: Comparison of enhancement effects at different MWNTs ratios and changes with temperature of (a)storage modulus, (b)loss modulus and (c)tanδ

The storage and loss modulus in viscoelastic materials measure the stored energy, representing the elastic portion, and the energy dissipated as heat, representing the viscous portion.

It is reported that with the CNTs load increasing, the storage modulus of the composites dramatically increases. This can be explained as the particle-particle interactions and particle-fluid interactions increase due to the cylindrical shape with high aspect ratio of CNTs. According to the DMA test by Song et al. [44] the well dispersed CNTs nanocomposites show better performance in tensile strength, storage modulus, loss modulus, and complex viscosity, which was explained that the agglomerates in the poorly dispersed CNTs act as large particles with the increase of the CNTs loading. What's more, the poorly dispersed CNTs exhibit stronger non-Newtonian behavior, which means it has, from a rheological point of view, a more solid-like behavior.

From the Figure 3.9 (a), it was obvious that with the embedded BPs, the storage modulus was improved compared with neat epoxy, regardless of the MWNTs concentration in BPs. Compared with 100% MWNTs BPs, the storage modulus decreased with the decrease of the MWNTs concentration, except when the concentration was between 66 - 75%. This indicated that BPs with MWNTs concentration around 66% achieved the best mechanical enhancement. The similar results also showed in loss modulus and tan δ that 66% MWNTs BPs had highest loss modulus and similar tan δ with 100% MWNTs but much lower than neat epoxy. This result was due to that the neat BPs were highly pores, as shown in Figure 3.10 (a). With the proper concentration of GN fillers, the particles filled certain space and made the network turn to be more compact, as shown in Figure 3.10 (b). This increased

the surface roughness which was a likely reason to enhance the fracture toughness and improved mechanical properties in nanocomposites by modifying the viscoelastic epoxy matrix. With the decrease of MWNTs concentration in BPs, the compact network of MWNTs got harder to form. GN particles entangled by MWNTs acted as big aggregates, as shown in Figure 3.10 (c), and negatively influenced the mechanical performance of BPs and furthermore the nanocomposites.

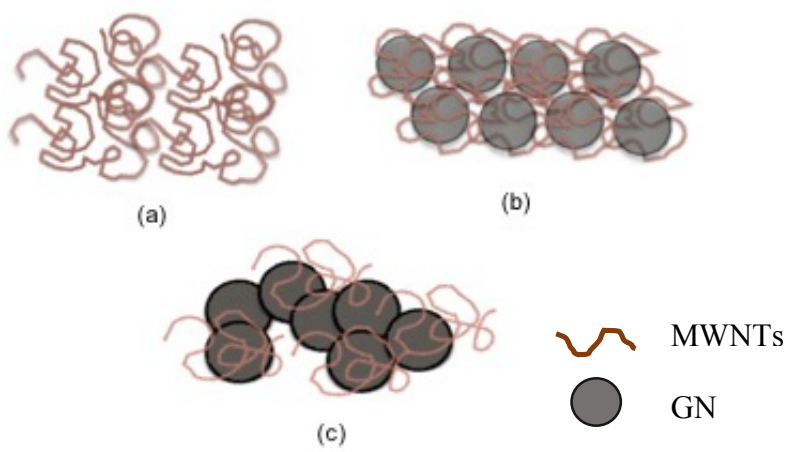

Figure 3.10: MWNTs/GN networks of (a) neat BPs, (b) 66% MWNTs BPs, and (c) low concentration MWNTs BPs.

Chapter 4:

Sensing function of BPs embedded nanocomposites

Introduction

From the research results mentioned in previous sections, CNTs possess the potential for electrical applications. Since the electronic bandgap changes have been computed by other researchers [100, 101] as a function of strain from compression, stretch, torsion and bending. Due to the property that CNTs' band structure on mechanical deformation, this chapter, the possibility to develop nanoelectromechanical sensors based on BPs would be demonstrated. The main objective of this chapter is to explore the strain-sensing capability of CNTs at the nanoscale to develop macroscale strain sensors based on the nanocomposite films.

The piezo-resistance response and sensing capability of the MWNTs-based and hybrid-based nanocomposite sensors were characterized by conducting various tensile tests. The main variables considered were: i) the membrane materials (neat MWNTs and hybrid MWNTs/GNs); ii) the load conditions (quasi-static and cyclic).

The quasi-static tests were applied to test the failure strain of the sensors at the high stresses and strains, whereas the cyclic loading was used to characterize the sensor response under repetitive straining.

4.1 Quasi-static loading

Due to the fragility and transferring strain to the tubes, developing BPs to

dynamic strain sensors for practical applications has been limited. There have been researches using Raman spectroscopy in both nano-scale and macro-scale. However, Raman spectroscopy is not practical in the field engineering limited by its complexity. In this work, since we embedded BPs into epoxy to protect BPs sensors and the nanocomposites transferred strain to the sensors so that this piezo-resistive strain sensor is simple and can be characterized and tested in the macro-scale.

Since the electronic conductivity had been measured using four-probe method in the last chapter, here the two-probe method was applied to measure the trend of electronic resistance changes responded to the deformation changes.

The quasi-static tests were carried out to assess the force and normalized resistance change upon the strain evolved until failure.

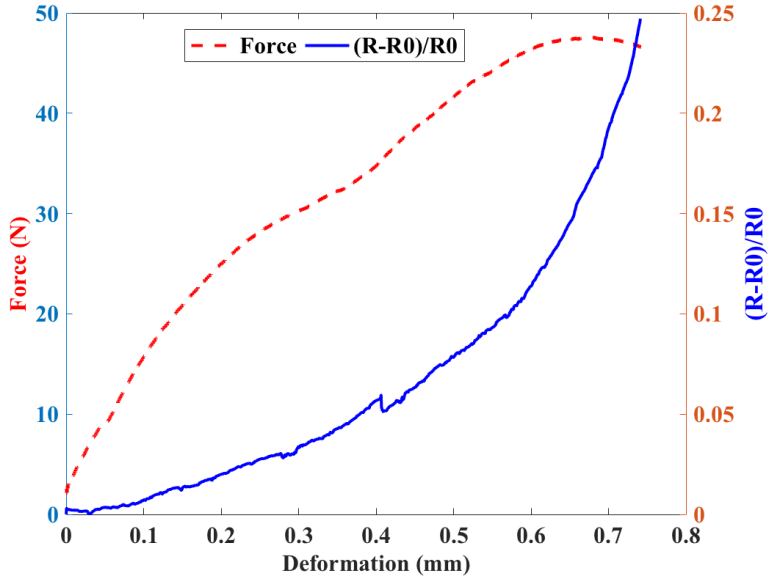

Figure 4.1: Piezoresistive repose of composite sensor until failure

Figure 4.2 showed the stable linear relationship between the change in electrical resistance and the strain. By changing the embedded BPs from neat BPs to hybrid BPs, the linear relationship remained.

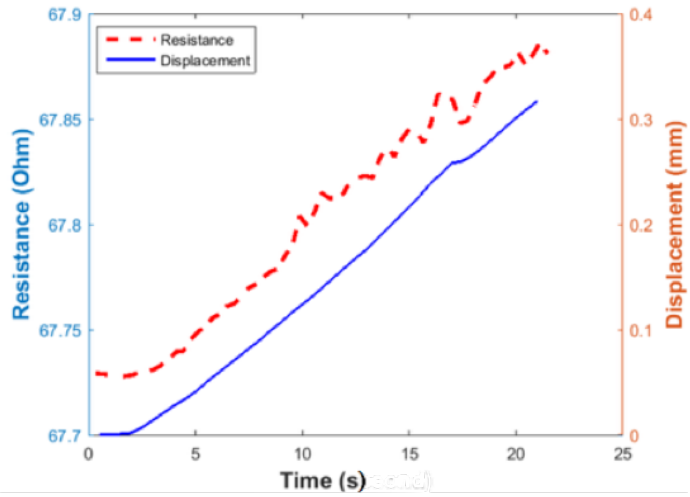

Figure 4.2: Linear relationship between change in resistance and strain

As shown in Figure 4.1, the composite sensor didn't function in the whole strain change range, mostly due to the BP failure, disruption of the conducting path and the plastic deformation of the epoxy, which resulted in an abrupt change in sensor resistance. As shown in Figure 4.2, in general, electrical resistance showed proportional linear response to the deformation under 0.4 mm. As the deformation went above 0.2 mm, noises in measured electrical resistance increased. These noises appeared probably because of the contact resistance among MWNTs, and MWNTs/GN networks [87] and the slip of the MWNTs and GN due to the weak Van der Waals force interactions at CNTs interfaces. According to the deduction of Kang et al. [102], ideally, the strain was supposed to transfer to the CNTs in the sensors. However, the slipping

between CNTs bundles may reduce the strain transferred through the composites, cause more noises, and degrade the sensitivity of the sensors over time.

As discussed in last chapter, deformation between 0 - 0.1 mm would be the ideal optimal deformation range, because the cold hardening and cramp could be significantly avoided. In the optimal range, composite showed elastic linear deformation responded to force applied. Put these results together to analysis, since the deformation elastic range was 0 - 0.1mm and in the same time, composites had a lower noise/signal ratio on the measure, we drew the conclusion that in our work, the optimal deformation range for the strain sensors will be 0 - 0.1 mm.

4.2 Cycle loading

The cyclic loading was used to characterize the sensor response under periodical forces.

The deformation and resistance changes as a function of time of the embedded BPs nanocomposites were shown in Figure 4.3. The electrical resistance of the sensors in the cyclic tests closely followed the strain data. These experimental results indicated the hybrid nanocomposites possessed sensing feature, which meant nanocomposite sensors were able to measure the strain in materials and the resistance changed linearly according to the strain changes.

The resistance changing as a function of strain of neat BPs sensors was similar to hybrid BPs sensors, which meant the mechanism controlling the electromechanical properties of both sensors was similar. In the work of Rein et al. [40], SWNTs BPs sensors also showed similar responses. All those results indicated that the intrinsic piezo-resistance properties of CNTs didn't involve a lot.

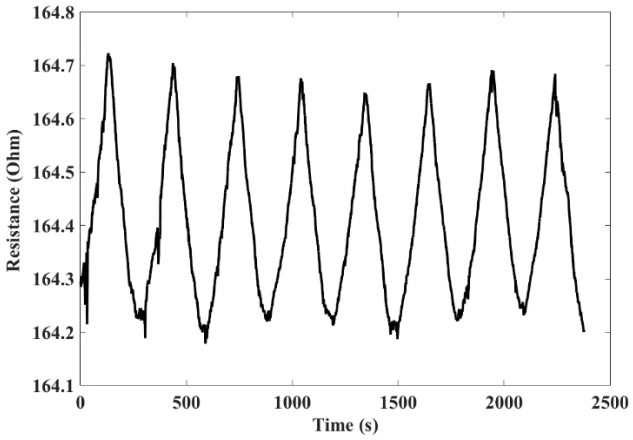

(a)

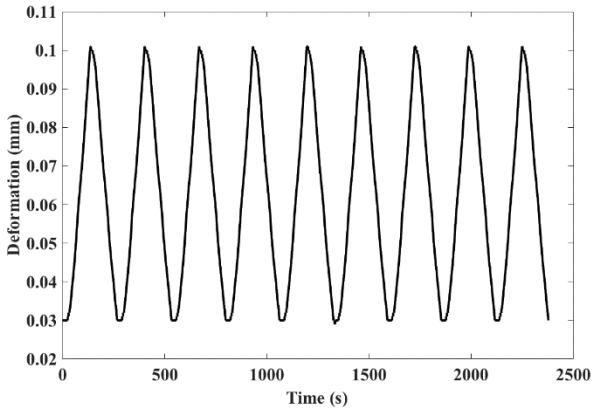

(b)

Figure 4.3: Resistance change responded to multi-cycle loading

Instead, the contact resistance between CNTs and tunneling resistance between particles got involved and may lead to exponential dependency. In spite of the exponential behavior of the BP sensor, the linear approximation was

still obtained and thus simplified the comparison, and showed the stable and regular electromechanical trend.

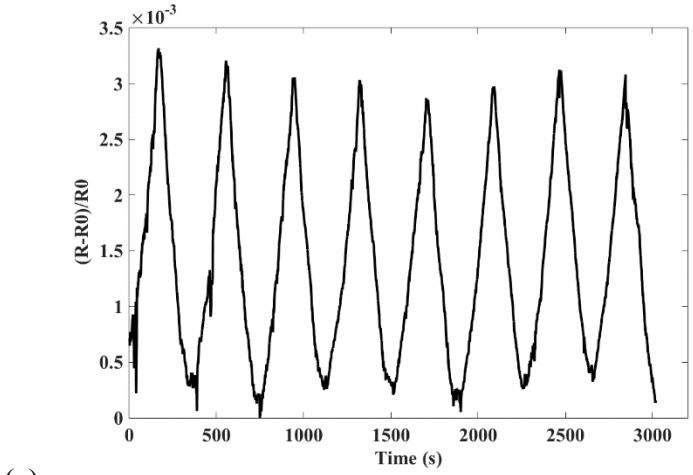

(a)

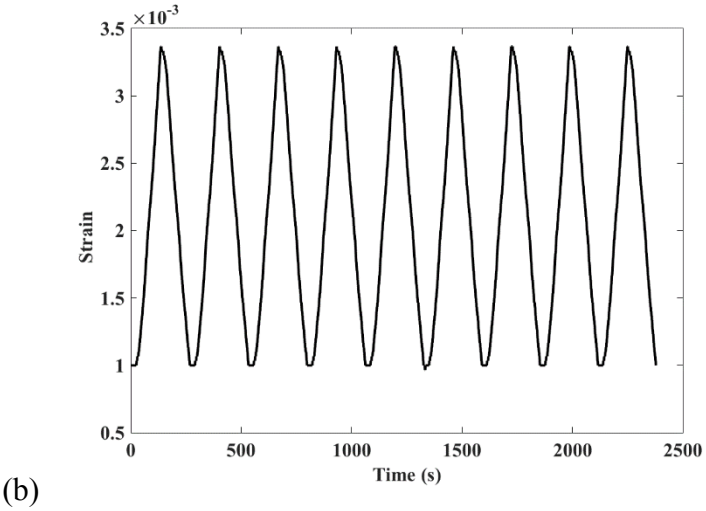

(b)

Figure 4.4: (a) Normalized resistance change; (b) strain cycle loading.

The typical strain sensitivity (Ss) is defined as:

$$Ss = \frac{(R-R0)/R0}{\varepsilon}$$ [50, 103]

where R is the measured resistance, R_0 is the nominal (i.e. no strain) resistance, and ε is the strain.

The normalized resistance change and strain cycle loading is shown in

Figure 4.4. The calculated sensitivity was 0.818 with the standard deviation 0.0975.

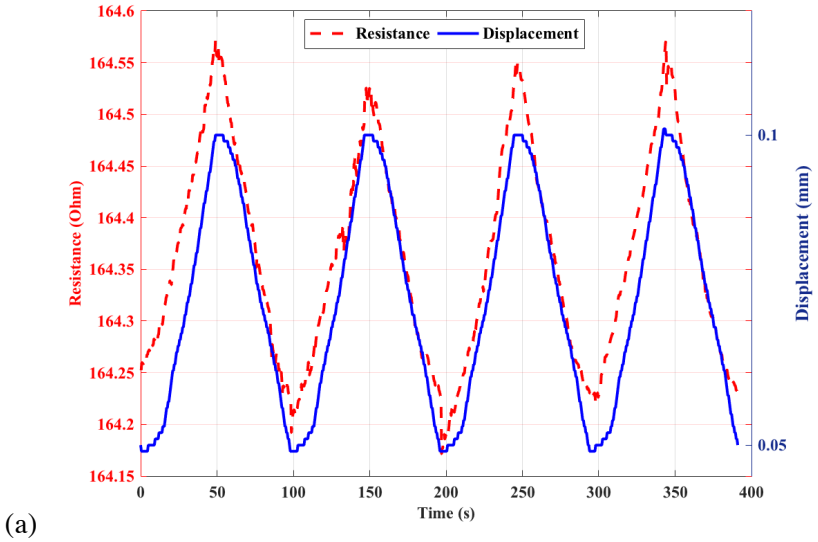

(a)

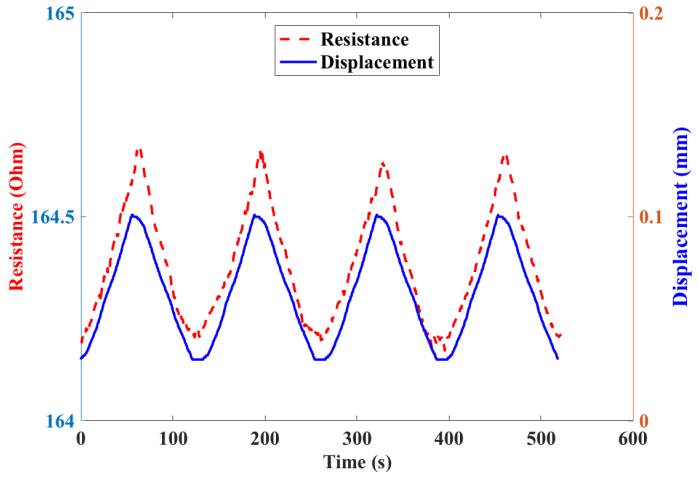

(b)

Figure 4.5: Resistance response to displacement when (a) large strain and (b) small strain applied

When different strain loading applied to the composites, as shown in Figure 4.5, the electrical resistance of the sensors in the cyclic tests followed the strain data, closely. These experimental results indicated the hybrid nanocomposites possessed sensing feature, which were able to measure strain changes in materials and the resistance changes linearly response to the strain.

The resistance changes in hybrid BPs nanocomposites with different strains were compared in Figure 4.6. This also indicated the real-time linear response of the sensors. From the results, the conclusion can be drawn as the nanocomposites can be used as strain sensor when strain was between 0.1 – 0.31%.

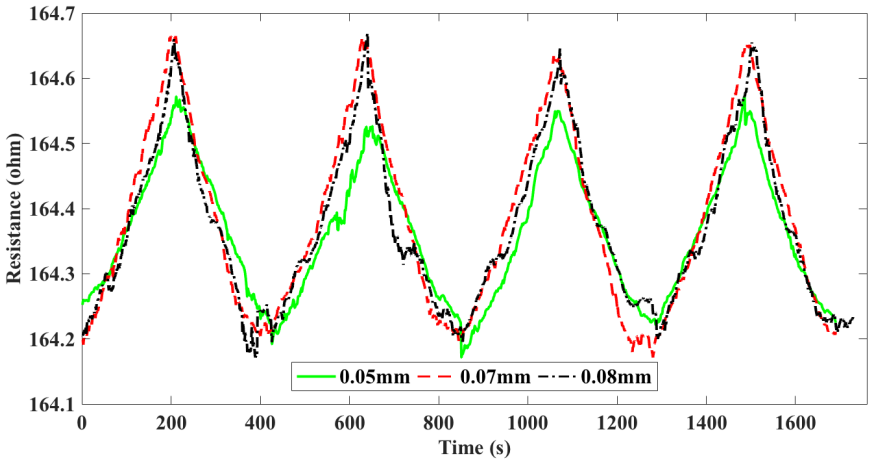

.

Figure 4.6: Electrical changes comparison under different deformation ranges.

Chapter 5:

Application and validation of BPs embedded nanocomposites

Introduction

In this chapter, the application and validation of nanocomposites were demonstrated.

The nanocomposites were attached to steel plates and aluminum plates to perform four-point bending test and tensile tests, using Instron. When four-point bending test was applied, the steel plate was cut into shape of rectangle. While when tensile test was applied, the aluminum plate was cut into shape of dog-bone.

The results of both tests showed the linear response of sensors to the strain changes. These results indicated that the nanocomposites can be used as strain sensors for small strain range.

5.1 Four-point bending test on nanocomposites

In this work, four-point bending tests were applied. Similar to the three-point bending test, the four-point bending test can provide values for the Young's modulus, flexural stress and flexural strain. Using the stress and strain response of the material, the strain-stress curve will be obtained. The major difference between these two methods is that the addition of a 4^{th} bearing brings a much larger portion of the beam to the maximum stress, as opposed to only the material right under the center bearing [104-106]. The other reason is to attach the sensor onto the center of a steel plate, the three-point bending is not

practical because the force will be applied to the sensor directly due to the contact at the center point. This contact has the risk to break the sensor and the sensing function results will be inaccurate. The scheme or a four-point bending test is shown in Figure 5.1.

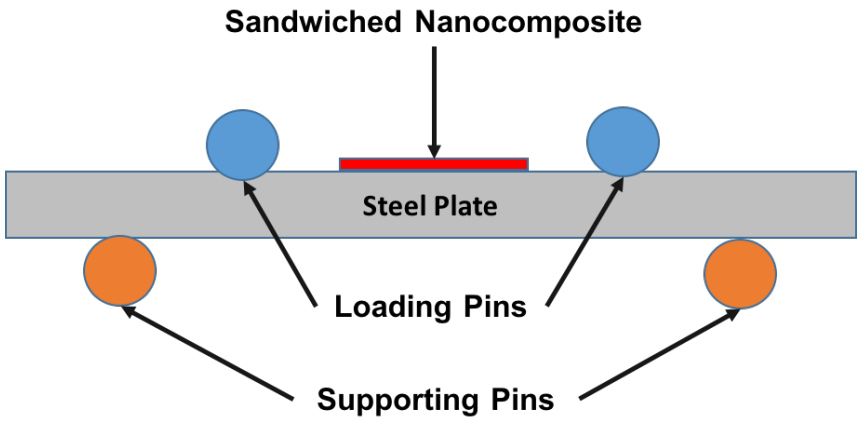

Figure 5.1: Four-point bending fixture scheme

The four-point bending test was carried out on Instron 8800 Series Servohydraulic Test System, which meets the International Electromagnetic Compatibility (EMC) standards.

The bending fixture is series 2810-181 with 100KN capacity. This fixture is the three-point bending fixture. Among all accessories, the 2810-184 is the matching conversion kit to convert a three-point bending fixture to a four-point bending fixture. Then attach the four-point bending fixture to the Instron 8800 machine.

The Instron 8800 material test system, as shown in Figure 5.2, is a very versatile piece of equipment and is widely used to study properties of different materials, like composites. This system can perform a variety of Tensile,

Compression, Flex, Cyclic, Creep and Relaxation type tests for different applications.

Figure 5.2: Four-point bending test setup on Instron

The data produced by the force gauge on the Instron 8800 test machine, an additional data acquisition system, and desktop computer were used. The data acquisition unit was mated to the sensor as well as plugged into a computer for control. The software "Bluehill 3" was developed to control and monitor tests, collect data, analyze and calculate results, produce graphs and generate reports. The system provided a fully automated experimental setup.

The nanocomposite film was attached to the steel plate by curing the epoxy between the sensor and the steel plate. The strain rate was 0.001/min. As shown

in Figure 5.3, the resistance of the nanocomposite sensor had the linear response to the strain change.

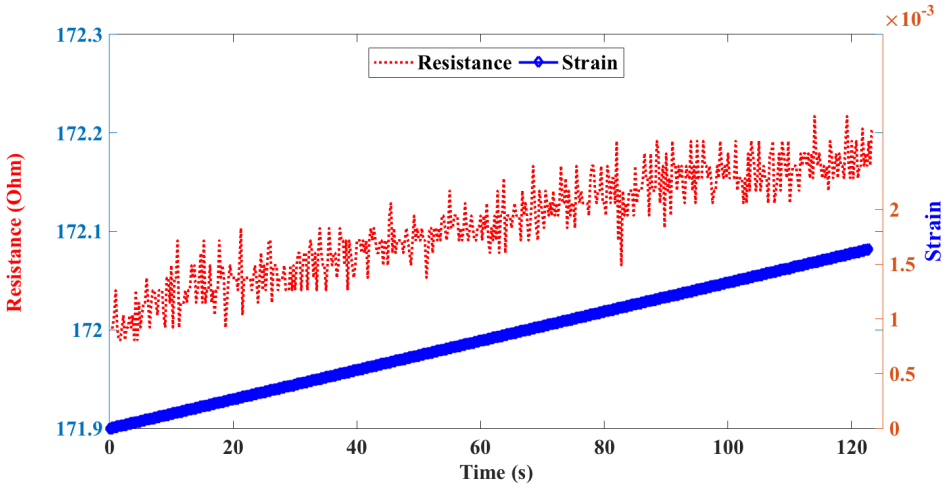

Figure 5.3: Linear relationship between change in resistance and strain

5.2 Tensile test on nanocomposite film

In the work of Thostenson et al. [107], their TEM pictures revealed the critical nanoscale buckling behavior of MWNTs in a nanotube reinforced nanocomposite. Since this behavior varied with the nanotube diameter, the larger diameter of CNTs, they showed segmental buckling at higher strain, which indicated continued transfer of load to the nanotubes after initial buckling. In tensile loading, the stress was carried out by the outer nanotube walls without being transferred to the interior walls. In bending load, the displacement of all nanotube wall was required, which leaded to higher flexural stiffness. Because the column buckling was a function of the flexural stiffness, MWNTs would show the increased resistance to the buckling. When it came to compression, the epoxy matrix supported MWNTs, and the overall buckling

behavior of MWNTs was further constrained. Without the constraint of the matrix, MWNTs may reach a larger-scale bending. The novel properties may not able to transfer in macroscopic scale in compression. Therefore, the tensile test is proper for CNTs tests rather than compression tests.

The tensile test was carried out by using Instron wedge action grips with 100 kN capacity. The wedge action grips held a test specimen between a stationary load frame member and force producing crosshead. The wedge action design allowed the grip faces to tighten onto a specimen without altering the vertical position of the faces in relation to the specimen. This allowed to install a test specimen without exerting a tensile preload on it.

The video extensometer, shown in Figure 5.4, was used to accurately measure specimen strain during the static tensile test without the need to contact the specimen. This method had the advantages, including no mechanical influence on the specimen, ease of use, and reproducibility. The principle of the video extensometer was based on accurate detection of the gauge length marker using a high resolution digital video camera. In this work, the length between white markers was one inch.

Figure 5.4: Video extensometer

The specimen was shaped as dog-bone for the tensile test, as shown in Figure 5.5. In tensile test, dog-bone shape is critical to the accurate results [108], because it prevents failure in the grips. Additionally, grips of tensile testing machines have teeth to achieve a sufficiently strong grip that can withstand the forces required to deform the sample longitudinally. The teeth typically cause plastic deformation of the gripped portion of the sample. The plastic deformation at the grips may change the material properties, and definitely changes the sample geometry. The sample geometry changes in such a way as to create stress concentrations in the gripped region. Both changes would contribute to an improper measurement if failure occurred at the grips in a cylindrical or bar specimen without enlarged ends. The gage length is the region over which measurements are made and is centered within the reduced section.

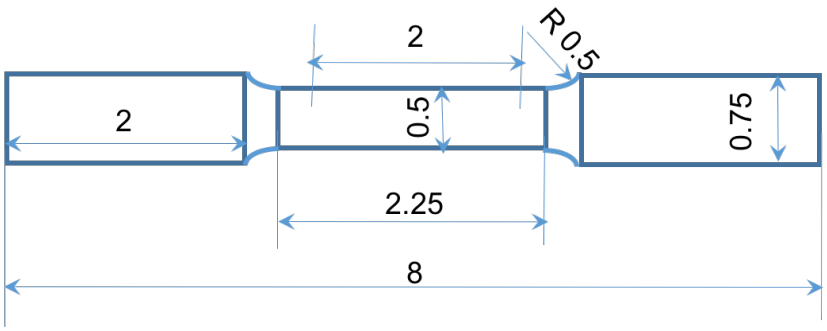

Figure 5.5: Geometry of the specimens for tensile testing, unit in inch

The specimen was made of 2024-T351 aluminum. The normal material thickness was 0.5 in. The geometry of specimens was shown in Figure 5.5 based on ASTM E8/E8M-13 [109, 110].

(a) (b)

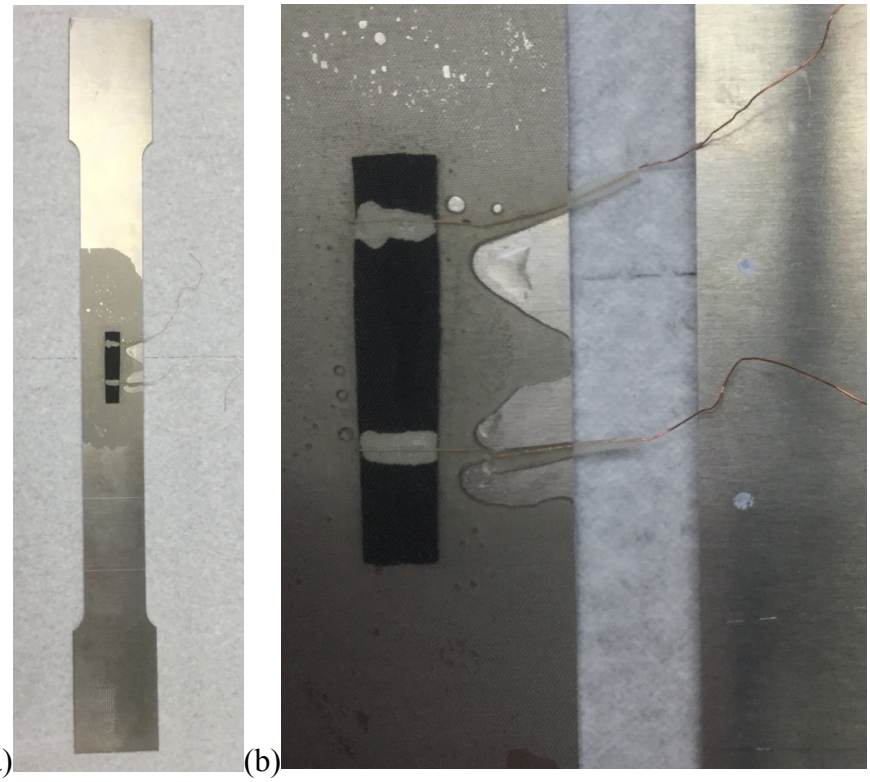

Figure 5.6: (a) Dog-bone specimen with the sensor attached, (b) with the dots draw on the back to measure the strain by extensometer

As shown in Figure 5.6, the dog-bone specimen with sensor attached and white dots drew on the back for the further strain measurement were prepared. The Instron electro-mechanical testing machine setup is shown in Figure 5.7. The static tensile test was performed at room temperature and at a constant rate of 0.5 mm/min.

(a) 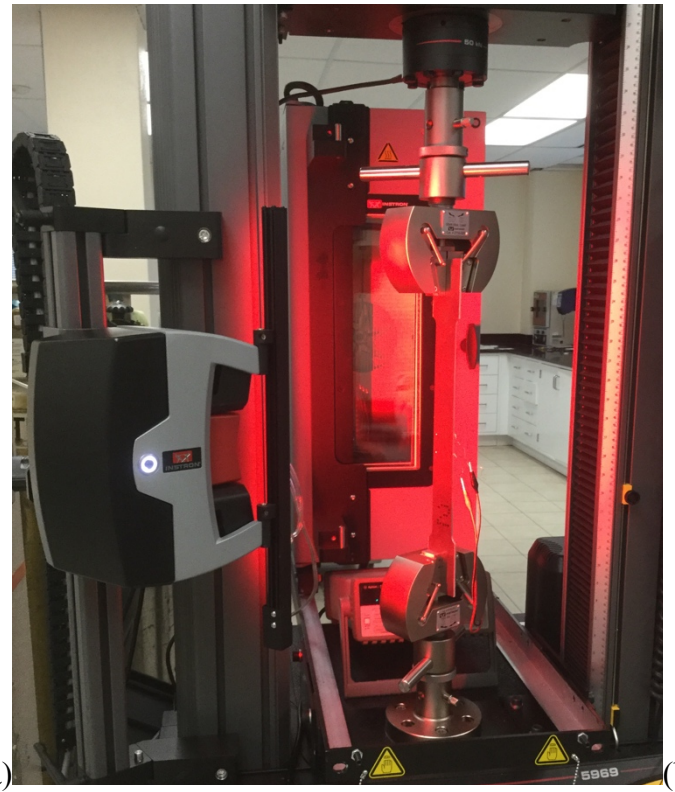 (b) 

Figure 5.7: Instron tensile test setup (a) front site where two white dots drew with the extensometer on, (b) back site where the sensor attached with the extensometer off.

Figure 5.8 showed the result of the tensile test. The strain increased linearly with the resistance responded linearly. The resistance increased stably with negligible noises. This results proved that the sensor can be applied to practical sensing applications, especially in use for small strain changes.

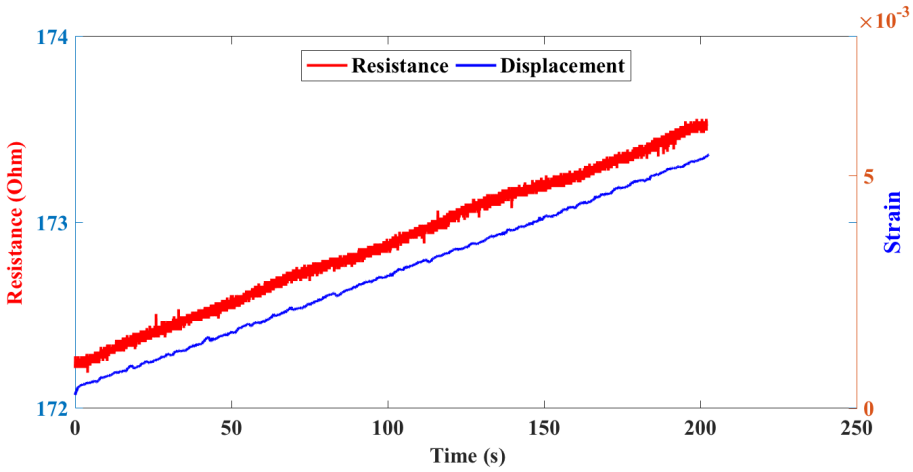

Figure 5.8: The linear response of resistance to the strain changes

The strain range increased to 5.1% and the calculated sensitivity could reach 1.4, which went even higher than the tensile test applied directly to the sensor. The dog-bone shaped aluminum contributed to higher strain range and increased sensitivity.

Chapter 6:

Summary and recommendations

6.1 Summary

In this work, fabrication, characterization and application of nanocomposites were demonstrated.

The efficient, easy and novel fabrication method for BP membranes without surfactant was developed. Based on this method, two main types of BPs fabricated, neat BPs and hybrid BPs made of MWNTs and GN. The threshold of hybrid BPs was also found as weight ratio of MWNTs in BPs above 25%. Nanocomposites were fabricated by embedding BPs core into epoxy coating. In this way, the epoxy coating can protect BPs sensors and uniformly transfer the strain to the entire composites so as to BPs sensors.

SEM was carried out to investigate the surface fine structure of BPs in nano-scale. Four-probe method was explored to measure the accurate conductivity of BPs. We drew the conclusion that the resistance of BPs was dominant by the contact resistance instead of the intrinsic resistance. The measured conductive resistance of neat MWNTs BPs was 302 S/m. DMA were implemented to test dynamic mechanical properties. The elastic deformation occurred when the strain was lower than 0.31 %. The mechanical properties were tested by tensile tests using the Micro Mechanical Testing Stage. Among all samples, hybrid BPs with 66 wt. % MWNTs showed the best mechanical performance and improvement.

To investigate the sensing function, quasi-static and cyclic loading tests were carried out. The optimal range for strain loading was 0.1 – 0.31 % while the sensitivity of the composite sensor could achieve 0.82 and showed the closely linear real-time response to the strain change. The dog-bone shaped aluminum contributed to uniform linear strain changes, which increased the strain range to 5.1% and sensitivity to 1.4. These results showed remarkable potential for BPs embedded nanocomposites to be used for strain sensing.

Besides, the detailed comparison of two-probe and four-probe method was addressed. In addition, the scenarios where four-probe method could perform better were analyzed, which may be valuable for researchers to choose proper measurement approaches.

6.2 Recommendations

For further investigation, polymers with different properties can be applied to replace the epoxy resin. Since the elastic properties of the polymer matrix have a significant influence on the mechanical properties of the composites, we recommend that thermoplastic polymers may have potential to be the better candidate to develop strain sensors with larger strain range and sensitivity.

Besides, the shape memory polymer has the outstanding potential to develop multi-functional composites with BPs embedded.

What's more, the further developed BPs sensors are supposed to be embedded in metals or composites plates to test their practical value in the field engineering.

References

1. Iijima, S. and T. Ichihashi, *Single-shell carbon nanotubes of 1-nm diameter.* 1993.
2. Treacy, M.M.J., T.W. Ebbesen, and J.M. Gibson, *Exceptionally high Young's modulus observed for individual carbon nanotubes.* Nature, 1996. **381**(6584): p. 678-680.
3. Allaoui, A., S. Bai, H.M. Cheng, and J.B. Bai, *Mechanical and electrical properties of a MWNT/epoxy composite.* Composites Science and Technology, 2002. **62**(15): p. 1993-1998.
4. Sandler, J.K.W., J.E. Kirk, I.A. Kinloch, M.S.P. Shaffer, and A.H. Windle, *Ultra-low electrical percolation threshold in carbon-nanotube-epoxy composites.* Polymer, 2003. **44**(19): p. 5893-5899.
5. Tombler, T.W., C. Zhou, L. Alexseyev, J. Kong, H. Dai, L. Liu, C.S. Jayanthi, M. Tang, and S.-Y. Wu, *Reversible electromechanical characteristics of carbon nanotubes under local-probe manipulation.* Nature, 2000. **405**(6788): p. 769-772.
6. Liang, Y., H. Zhang, B. Yi, Z. Zhang, and Z. Tan, *Preparation and characterization of multi-walled carbon nanotubes supported PtRu catalysts for proton exchange membrane fuel cells.* Carbon, 2005. **43**(15): p. 3144-3152.
7. Thostenson, E.T., Z. Ren, and T.-W. Chou, *Advances in the science and technology of carbon nanotubes and their composites: a review.* Composites science and technology, 2001. **61**(13): p. 1899-1912.
8. Iijima, S., *Carbon nanotubes: past, present, and future.* Physica B: Condensed Matter, 2002. **323**(1–4): p. 1-5.
9. Hill, C.B., *Investigation of electrical and impact properties of carbon fiber reinforced polymer matrix composites with carbon nanotube buckypaper layers.* 2012.
10. Popov, V., V. Van Doren, and M. Balkanski, *Lattice dynamics of single-walled carbon nanotubes.* Physical Review B, 1999. **59**(13): p. 8355.
11. Popov, V.N., V.E. Van Doren, and M. Balkanski, *Elastic properties of crystals of single-walled carbon nanotubes.* Solid State Communications, 2000. **114**(7): p. 395-399.
12. Lu, J.P., *Elastic properties of single and multilayered nanotubes.* Journal of Physics and Chemistry of Solids, 1997. **58**(11): p. 1649-1652.
13. Yu, M.-F., O. Lourie, M.J. Dyer, K. Moloni, T.F. Kelly, and R.S. Ruoff, *Strength and breaking mechanism of multiwalled carbon nanotubes under tensile load.* Science, 2000. **287**(5453): p. 637-640.
14. Chico, L., V.H. Crespi, L.X. Benedict, S.G. Louie, and M.L. Cohen, *Pure Carbon Nanoscale Devices: Nanotube Heterojunctions.* Physical Review Letters, 1996. **76**(6): p. 971-974.

15. Crespi, V.H., L.X. Benedict, M.L. Cohen, and S.G. Louie, *Prediction of a pure-carbon planar covalent metal.* Physical Review B, 1996. **53**(20): p. R13303-R13305.
16. Crespi, V.H., M.L. Cohen, and A. Rubio, *In situ band gap engineering of carbon nanotubes.* Physical review letters, 1997. **79**(11): p. 2093.
17. Kane, C.L. and E. Mele, *Size, shape, and low energy electronic structure of carbon nanotubes.* Physical Review Letters, 1997. **78**(10): p. 1932.
18. Rochefort, A., D.R. Salahub, and P. Avouris, *The effect of structural distortions on the electronic structure of carbon nanotubes.* Chemical Physics Letters, 1998. **297**(1): p. 45-50.
19. Tans, S.J., M.H. Devoret, H. Dai, A. Thess, R.E. Smalley, L. Georliga, and C. Dekker, *Individual single-wall carbon nanotubes as quantum wires.* Nature 386 (6624), 474-477.(1997), 1997.
20. Bezryadin, A., A. Verschueren, S. Tans, and C. Dekker, *Multiprobe transport experiments on individual single-wall carbon nanotubes.* Physical Review Letters, 1998. **80**(18): p. 4036.
21. Langer, L., V. Bayot, E. Grivei, J.P. Issi, J.P. Heremans, C.H. Olk, L. Stockman, C. Van Haesendonck, and Y. Bruynseraede, *Quantum Transport in a Multiwalled Carbon Nanotube.* Physical Review Letters, 1996. **76**(3): p. 479-482.
22. Bockrath, M., D.H. Cobden, P.L. McEuen, N.G. Chopra, A. Zettl, A. Thess, and R.E. Smalley, *Single-electron transport in ropes of carbon nanotubes.* Science, 1997. **275**(5308): p. 1922-1925.
23. Paulson, S., M. Falvo, N. Snider, A. Helser, T. Hudson, A. Seeger, R. Taylor, R. Superfine, and S. Washburn, *In situ resistance measurements of strained carbon nanotubes.* Applied Physics Letters, 1999. **75**(19): p. 2936-2938.
24. Nardelli, M.B. and J. Bernholc, *Mechanical deformations and coherent transport in carbon nanotubes.* Physical Review B, 1999. **60**(24): p. R16338-R16341.
25. Yu, X. and E. Kwon, *Carbon Nanotube Based Self-sensing Concrete for Pavement Structural Health Monitoring*. 2012, Research report– Univ of Minnesota Duluth, Contract Number: US DOT: DTFH61-10-C-00011.
26. Hashmi, S.A.R., H.C. Prasad, R. Abishera, H.N. Bhargaw, and A. Naik, *Improved recovery stress in multi-walled-carbon-nanotubes reinforced polyurethane.* Materials & Design, 2015. **67**: p. 492-500.
27. Moniruzzaman, M. and K.I. Winey, *Polymer Nanocomposites Containing Carbon Nanotubes.* Macromolecules, 2006. **39**(16): p. 5194-5205.
28. Han, B., S. Sun, S. Ding, L. Zhang, X. Yu, and J. Ou, *Review of nanocarbon-engineered multifunctional cementitious composites.*

Composites Part A: Applied Science and Manufacturing, 2015. **70**: p. 69-81.
29. Rana, S., R. Alagirusamy, and M. Joshi, *A review on carbon epoxy nanocomposites.* Journal of Reinforced Plastics and Composites, 2008.
30. Kumar, K.S., R. Biju, and C.R. Nair, *Progress in shape memory epoxy resins.* Reactive and Functional Polymers, 2013. **73**(2): p. 421-430.
31. X. F. Xie, L.G., J. Sun,, *Esterification of Chemical Functional Single-Wall Carbon Nanotubes.* Materials Science Forum, 2011. **695**: p. 373-376.
32. Yan, Y., J. Cui, S. Zhao, J. Zhang, J. Liu, and J. Cheng, *Interface molecular engineering of single-walled carbon nanotube/epoxy composites.* Journal of Materials Chemistry, 2012. **22**(5): p. 1928-1936.
33. Felisberto, M., A. Arias-Durán, J.A. Ramos, I. Mondragon, R. Candal, S. Goyanes, and G.H. Rubiolo, *Influence of filler alignment in the mechanical and electrical properties of carbon nanotubes/epoxy nanocomposites.* Physica B: Condensed Matter, 2012. **407**(16): p. 3181-3183.
34. Ramasubramaniam, R., J. Chen, and H. Liu, *Homogeneous carbon nanotube/polymer composites for electrical applications.* Applied Physics Letters, 2003. **83**(14): p. 2928-2930.
35. Baoguo, H., Y. Xun, and K. Eil, *A self-sensing carbon nanotube/cement composite for traffic monitoring.* Nanotechnology, 2009. **20**(44): p. 445501.
36. Sandler, J., M. Shaffer, T. Prasse, W. Bauhofer, K. Schulte, and A. Windle, *Development of a dispersion process for carbon nanotubes in an epoxy matrix and the resulting electrical properties.* Polymer, 1999. **40**(21): p. 5967-5971.
37. Xie, X.-L., Y.-W. Mai, and X.-P. Zhou, *Dispersion and alignment of carbon nanotubes in polymer matrix: A review.* Materials Science and Engineering: R: Reports, 2005. **49**(4): p. 89-112.
38. Guadagno, L., B. De Vivo, A. Di Bartolomeo, P. Lamberti, A. Sorrentino, V. Tucci, L. Vertuccio, and V. Vittoria, *Effect of functionalization on the thermo-mechanical and electrical behavior of multi-wall carbon nanotube/epoxy composites.* Carbon, 2011. **49**(6): p. 1919-1930.
39. Li, C., E.T. Thostenson, and T.-W. Chou, *Dominant role of tunneling resistance in the electrical conductivity of carbon nanotube–based composites.* Applied Physics Letters, 2007. **91**(22): p. 223114.
40. Rein, M.D., O. Breuer, and H.D. Wagner, *Sensors and sensitivity: Carbon nanotube buckypaper films as strain sensing devices.* Composites Science and Technology, 2011. **71**(3): p. 373-381.
41. Kim, Y.A., H. Muramatsu, T. Hayashi, M. Endo, M. Terrones, and M.S. Dresselhaus, *Fabrication of High-Purity, Double-Walled Carbon*

Nanotube Buckypaper. Chemical Vapor Deposition, 2006. **12**(6): p. 327-330.
42. Ding, W., S. Pengcheng, L. Changhong, W. Wei, and F. Shoushan, *Highly oriented carbon nanotube papers made of aligned carbon nanotubes.* Nanotechnology, 2008. **19**(7): p. 075609.
43. Pötschke, P., N.P. Zschoerper, B.P. Moller, and U. Vohrer, *Plasma Functionalization of Multiwalled Carbon Nanotube Bucky Papers and the Effect on Properties of Melt-Mixed Composites with Polycarbonate.* Macromolecular rapid communications, 2009. **30**(21): p. 1828-1833.
44. Song, Y.S. and J.R. Youn, *Influence of dispersion states of carbon nanotubes on physical properties of epoxy nanocomposites.* Carbon, 2005. **43**(7): p. 1378-1385.
45. Kinloch, I.A., S.A. Roberts, and A.H. Windle, *A rheological study of concentrated aqueous nanotube dispersions.* Polymer, 2002. **43**(26): p. 7483-7491.
46. Spitalsky, Z., D. Tasis, K. Papagelis, and C. Galiotis, *Carbon nanotube–polymer composites: Chemistry, processing, mechanical and electrical properties.* Progress in Polymer Science, 2010. **35**(3): p. 357-401.
47. Ting, Z., *Preparation and Performance of Buckypapers Based on Carbon Nanotubes*, in *Materials Science*. 2013, Harbin Engineering University.
48. Hussein, L., G. Urban, and M. Kruger, *Fabrication and characterization of buckypaper-based nanostructured electrodes as a novel material for biofuel cell applications.* Physical Chemistry Chemical Physics, 2011. **13**(13): p. 5831-5839.
49. Vohrer, U., I. Kolaric, M.H. Haque, S. Roth, and U. Detlaff-Weglikowska, *Carbon nanotube sheets for the use as artificial muscles.* Carbon, 2004. **42**(5–6): p. 1159-1164.
50. Loh, K.J., T.-C. Hou, J.P. Lynch, and N.A. Kotov, *Carbon Nanotube Sensing Skins for Spatial Strain and Impact Damage Identification.* Journal of Nondestructive Evaluation, 2009. **28**(1): p. 9-25.
51. Zhang, C.-S., Q.-Q. Ni, S.-Y. Fu, and K. Kurashiki, *Electromagnetic interference shielding effect of nanocomposites with carbon nanotube and shape memory polymer.* Composites Science and Technology, 2007. **67**(14): p. 2973-2980.
52. Jin Gyu, P., L. Jeffrey, C. Qunfeng, B. Jianwen, S. Jesse, L. Richard, W. Ben, Z. Chuck, S.B. James, K. Leslie, F. Percy, and D. David, *Electromagnetic interference shielding properties of carbon nanotube buckypaper composites.* Nanotechnology, 2009. **20**(41): p. 415702.
53. Wang, Z., Z. Liang, B. Wang, C. Zhang, and L. Kramer, *Processing and property investigation of single-walled carbon nanotube (SWNT)*

buckypaper/epoxy resin matrix nanocomposites. Composites Part A: Applied Science and Manufacturing, 2004. **35**(10): p. 1225-1232.
54. Koerner, H., G. Price, N.A. Pearce, M. Alexander, and R.A. Vaia, *Remotely actuated polymer nanocomposites--stress-recovery of carbon-nanotube-filled thermoplastic elastomers.* Nat Mater, 2004. **3**(2): p. 115-20.
55. Sahoo, N.G., Y.C. Jung, N.S. Goo, and J.W. Cho, *Conducting Shape Memory Polyurethane-Polypyrrole Composites for an Electroactive Actuator.* Macromolecular Materials and Engineering, 2005. **290**(11): p. 1049-1055.
56. Muramatsu, H., T. Hayashi, Y.A. Kim, D. Shimamoto, Y.J. Kim, K. Tantrakarn, M. Endo, M. Terrones, and M.S. Dresselhaus, *Pore structure and oxidation stability of double-walled carbon nanotube-derived bucky paper.* Chemical Physics Letters, 2005. **414**(4–6): p. 444-448.
57. Yeh, C.-S., *A study of nanostructure and properties of mixed nanotube buckypaper materials: Fabrication, process modeling characterization, and property modeling.* 2007.
58. Liu Yan, L.M., Liu Qianli, GU Yizhuo, Li Yanxia, Zhang Zuoguang, *Influence factors on the tensile properties of MWCNT buckypaper/epoxy composites.* Acta Materiae Compositae Sinica, 2012. **29**(6): p. 26-31.
59. Han, J.-H., H. Zhang, M.-J. Chen, G.-R. Wang, and Z. Zhang, *CNT buckypaper/thermoplastic polyurethane composites with enhanced stiffness, strength and toughness.* Composites Science and Technology, 2014. **103**: p. 63-71.
60. Li, J., Y. Gao, W. Ma, L. Liu, Z. Zhang, Z. Niu, Y. Ren, X. Zhang, Q. Zeng, H. Dong, D. Zhao, L. Cai, W. Zhou, and S. Xie, *High performance, freestanding and superthin carbon nanotube/epoxy nanocomposite films.* Nanoscale, 2011. **3**(9): p. 3731-3736.
61. Khan, U., I. O'Connor, Y.K. Gun'ko, and J.N. Coleman, *The preparation of hybrid films of carbon nanotubes and nano-graphite/graphene with excellent mechanical and electrical properties.* Carbon, 2010. **48**(10): p. 2825-2830.
62. Dharap, P., Z. Li, S. Nagarajaiah, and E. Barrera, *Nanotube film based on single-wall carbon nanotubes for strain sensing.* Nanotechnology, 2004. **15**(3): p. 379.
63. Dumée, L.F., K. Sears, J. Schütz, N. Finn, C. Huynh, S. Hawkins, M. Duke, and S. Gray, *Characterization and evaluation of carbon nanotube Bucky-Paper membranes for direct contact membrane distillation.* Journal of Membrane Science, 2010. **351**(1–2): p. 36-43.
64. Feng, Q.-P., J.-P. Yang, S.-Y. Fu, and Y.-W. Mai, *Synthesis of carbon nanotube/epoxy composite films with a high nanotube loading by a*

mixed-curing-agent assisted layer-by-layer method and their electrical conductivity. Carbon, 2010. **48**(7): p. 2057-2062.
65. Tsai, S.-Y., *Experimental study and modeling of nanotube buckypaper composite actuator for morphing structure applications.* 2016.
66. Pötschke, P., T.D. Fornes, and D.R. Paul, *Rheological behavior of multiwalled carbon nanotube/polycarbonate composites.* Polymer, 2002. **43**(11): p. 3247-3255.
67. Shenoy, A.V., *Rheology of filled polymer systems*. 2013: Springer Science & Business Media.
68. Zhu, J., J. Kim, H. Peng, J.L. Margrave, V.N. Khabashesku, and E.V. Barrera, *Improving the dispersion and integration of single-walled carbon nanotubes in epoxy composites through functionalization.* Nano letters, 2003. **3**(8): p. 1107-1113.
69. Yeh, C.-S., *A study of nanostructure and properties of mixed nanotube buckypaper materials: fabrication, process modeling characterization, and property modeling*. 2007: ProQuest.
70. Datsyuk, V., M. Kalyva, K. Papagelis, J. Parthenios, D. Tasis, A. Siokou, I. Kallitsis, and C. Galiotis, *Chemical oxidation of multiwalled carbon nanotubes.* Carbon, 2008. **46**(6): p. 833-840.
71. Xia, W., C. Jin, S. Kundu, and M. Muhler, *A highly efficient gas-phase route for the oxygen functionalization of carbon nanotubes based on nitric acid vapor.* Carbon, 2009. **47**(3): p. 919-922.
72. Darmstadt, H., C. Roy, S. Kaliaguine, J.-M. Ting, and R.L. Alig, *Surface spectroscopic analysis of vapour grown carbon fibres prepared under various conditions.* Carbon, 1998. **36**(7): p. 1183-1190.
73. Benlikaya, R., P. Slobodian, and P. Riha, *Enhanced strain-dependent electrical resistance of polyurethane composites with embedded oxidized multiwalled carbon nanotube networks.* J. Nanomaterials, 2013. **2013**: p. 8-8.
74. Xia, W., O.F.K. Schlüter, C. Liang, M.W.E. van den Berg, M. Guraya, and M. Muhler, *The synthesis of structured Pd/C hydrogenation catalysts by the chemical vapor deposition of Pd(allyl)Cp onto functionalized carbon nanotubes anchored to vapor grown carbon microfibers.* Catalysis Today, 2005. **102–103**: p. 34-39.
75. Jiang, Q., Y. Li, J. Xie, J. Sun, D. Hui, and Y. Qiu, *Plasma functionalization of bucky paper and its composite with phenylethynyl-terminated polyimide.* Composites Part B: Engineering, 2013. **45**(1): p. 1275-1281.
76. Pötschke, P., N.P. Zschoerper, B.P. Moller, and U. Vohrer, *Plasma Functionalization of Multiwalled Carbon Nanotube Bucky Papers and the Effect on Properties of Melt-Mixed Composites with Polycarbonate.* Macromolecular Rapid Communications, 2009. **30**(21): p. 1828-1833.

77. Lau, C.H., R. Cervini, S.R. Clarke, M.G. Markovic, J.G. Matisons, S.C. Hawkins, C.P. Huynh, and G.P. Simon, *The effect of functionalization on structure and electrical conductivity of multi-walled carbon nanotubes.* Journal of Nanoparticle Research, 2008. **10**(1): p. 77-88.
78. Inpil, K., J.S. Mark, H.K. Jay, S. Vesselin, and S. Donglu, *A carbon nanotube strain sensor for structural health monitoring.* Smart Materials and Structures, 2006. **15**(3): p. 737.
79. Hussein, L., S. Rubenwolf, F. von Stetten, G. Urban, R. Zengerle, M. Krueger, and S. Kerzenmacher, *A highly efficient buckypaper-based electrode material for mediatorless laccase-catalyzed dioxygen reduction.* Biosensors and Bioelectronics, 2011. **26**(10): p. 4133-4138.
80. Park, J.G., J. Smithyman, C.-Y. Lin, A. Cooke, A.W. Kismarahardja, S. Li, R. Liang, J.S. Brooks, C. Zhang, and B. Wang, *Effects of surfactants and alignment on the physical properties of single-walled carbon nanotube buckypaper.* Journal of Applied Physics, 2009. **106**(10): p. 104310.
81. Liu, D., Y. Liu, and G. Sui, *Synthesis and properties of sandwiched films of epoxy resin and graphene/cellulose nanowhiskers paper.* Composites Part A: Applied Science and Manufacturing, 2016. **84**: p. 87-95.
82. Hussein, L., G. Urban, and M. Krüger, *Fabrication and characterization of buckypaper-based nanostructured electrodes as a novel material for biofuel cell applications.* Physical Chemistry Chemical Physics, 2011. **13**(13): p. 5831-5839.
83. Dumée, L., V. Germain, K. Sears, J. Schütz, N. Finn, M. Duke, S. Cerneaux, D. Cornu, and S. Gray, *Enhanced durability and hydrophobicity of carbon nanotube bucky paper membranes in membrane distillation.* Journal of Membrane Science, 2011. **376**(1–2): p. 241-246.
84. *High-Speed Surfactant-Free Fabrication of Large Carbon Nanotube Membranes for Multifunctional Composites.* Journal of Aerospace Engineering, 2016. **29**(3): p. 04015060.
85. Pope, A.L., R.T. Littleton, and T.M. Tritt, *Apparatus for the rapid measurement of electrical transport properties for both "needle-like" and bulk materials.* Review of Scientific Instruments, 2001. **72**(7): p. 3129-3131.
86. Pope, A.L., B. Zawilski, and T.M. Tritt, *Description of removable sample mount apparatus for rapid thermal conductivity measurements.* Cryogenics, 2001. **41**(10): p. 725-731.
87. Xun, Y. and K. Eil, *A carbon nanotube/cement composite with piezoresistive properties.* Smart Materials and Structures, 2009. **18**(5): p. 055010.

88. Ping Ji, S.X., Larry Olson, *Experimental Organic Chemistry*. 2005, Bei Jing: Science Press.
89. Linda Paar, J.E., Kirk Manfredi, *Organic chemistry laboratory experiments for organic chemistry laboratory*. 2008.
90. Schadler, L.S., S.C. Giannaris, and P.M. Ajayan, *Load transfer in carbon nanotube epoxy composites.* Applied Physics Letters, 1998. **73**(26): p. 3842-3844.
91. Kakade, B.A., V.K. Pillai, D.J. Late, P.G. Chavan, F.J. Sheini, M.A. More, and D.S. Joag, *High current density, low threshold field emission from functionalized carbon nanotube bucky paper.* Applied Physics Letters, 2010. **97**(7): p. 073102.
92. Samal, M., P. Mohapatra, R. Subbiah, C.-L. Lee, B. Anass, J.A. Kim, T. Kim, and D.K. Yi, *InP/ZnS–graphene oxide and reduced graphene oxide nanocomposites as fascinating materials for potential optoelectronic applications.* Nanoscale, 2013. **5**(20): p. 9793-9805.
93. Kuphaldt, T.R., *Lessons in Electric Circuits* Vol. Vol. I - Direct Current (DC). EETech Media, LLC.
94. Jiang, G. *Four-probe resistance measurement*. 2009 2015; Available from: http://baike.baidu.com/view/2282469.htm.
95. Janesch, J. *Two-Wire vs. Four-Wire Resistance Measurements: Which Configuration Makes Sense for Your Application?* May 2013.
96. Yang, K., J. He, P. Puneet, Z. Su, M.J. Skove, J. Gaillard, T.M. Tritt, and A.M. Rao, *Tuning electrical and thermal connectivity in multiwalled carbon nanotube buckypaper.* Journal of Physics: Condensed Matter, 2010. **22**(33): p. 334215.
97. *Creep (deformation)*, in *Wikipedia*. 2016.
98. *Stress relaxation*, in *Wikipedia*. 2015.
99. *DMA Q Series Getting Started Guide*, T.I.-W. LLC, Editor. 2007.
100. Yang, L. and J. Han, *Electronic structure of deformed carbon nanotubes.* Physical Review Letters, 2000. **85**(1): p. 154.
101. Tombler, T.W., C. Zhou, L. Alexseyev, J. Kong, H. Dai, L. Liu, C. Jayanthi, M. Tang, and S.-Y. Wu, *Reversible electromechanical characteristics of carbon nanotubes under local-probe manipulation.* Nature, 2000. **405**(6788): p. 769-772.
102. Kang, I., Y.Y. Heung, J.H. Kim, J.W. Lee, R. Gollapudi, S. Subramaniam, S. Narasimhadevara, D. Hurd, G.R. Kirikera, V. Shanov, M.J. Schulz, D. Shi, J. Boerio, S. Mall, and M. Ruggles-Wren, *Introduction to carbon nanotube and nanofiber smart materials.* Composites Part B: Engineering, 2006. **37**(6): p. 382-394.
103. Akinwande Jr, A.I., *Nanocomposite strain sensors: Study of electrical and thermal properties*. 2007, Rice University.
104. Bending, A.D.S.T.M.f.F.P.o.U.a.R.P.a.E.I.M.b.F.-P.
105. *ASTM C1161: Standard Test Method for Flexural Strength of Advanced Ceramics at Ambient Temperature.*

106. Pais, J.C. and J. Harvey, *Four point bending*. 2012: CRC Press.
107. Thostenson, E.T. and T.-W. Chou, *Nanotube buckling in aligned multi-wall carbon nanotube composites.* Carbon, 2004. **42**(14): p. 3015-3018.
108. Davis, J.R., *Tensile testing*. 2004: ASM international.
109. E8/E8M-13, A., *Standard Test Methods for Tension Testing of Metallic Materials.* 2013.
110. Committee, A.I.H. and G.F. Vander Voort, *ASM handbook*. Vol. 9. 2004: Asm International Materials Park, OH.